



HAL
open science

Thermal and mechanical characterization of adobes bio-sourced with Pennisetum setaceum fibers and an application for modern buildings

Mouatassim Charai, Morad Salhi, Othmane Horma, Ahmed Mezrhab,
Mustapha Karkri, Samir Amraqui

► To cite this version:

Mouatassim Charai, Morad Salhi, Othmane Horma, Ahmed Mezrhab, Mustapha Karkri, et al.. Thermal and mechanical characterization of adobes bio-sourced with Pennisetum setaceum fibers and an application for modern buildings. *Construction and Building Materials*, 2022, 326, pp.126809. 10.1016/j.conbuildmat.2022.126809 . hal-04316664

HAL Id: hal-04316664

<https://hal.u-pec.fr/hal-04316664>

Submitted on 22 Jul 2024

HAL is a multi-disciplinary open access archive for the deposit and dissemination of scientific research documents, whether they are published or not. The documents may come from teaching and research institutions in France or abroad, or from public or private research centers.

L'archive ouverte pluridisciplinaire **HAL**, est destinée au dépôt et à la diffusion de documents scientifiques de niveau recherche, publiés ou non, émanant des établissements d'enseignement et de recherche français ou étrangers, des laboratoires publics ou privés.



Distributed under a Creative Commons Attribution - NonCommercial 4.0 International License

1 **Title**

2 Thermal and mechanical characterization of adobes bio-sourced with *Pennisetum setaceum*
3 fibers and an application for modern buildings

4 **Authors**

5 Mouatassim Charai^{1, 2, *}, Morad Salhi¹, Othmane Horma¹, Ahmed Mezrhab¹, Mustapha Karkri²,
6 Samir Amraqui¹

7 **Affiliations**

8 ¹ Mohammed First University, Mechanics and Energy Laboratory, 60000 Oujda, Morocco.

9 ² Université Paris- Est, CERTES, 61 Av. du Général de Gaulle, 94010 Créteil Cedex, France.

10 **E-mail:**

11 Mouatassim Charai: charai.m@yahoo.com, mouatassim.charai@u-pec.fr

12 *** Corresponding author**

13 E-mail: charai.m@yahoo.com; Mobile: +212(6)62300180

14 **Credit Author Statement**

15 **Mouatassim Charai:** Conceptualization, Methodology, Laboratory tests, Sample preparation,
16 Formal analysis, Investigation, Resources, Simulation, Visualization, Writing - original draft,
17 Writing - review & editing. **Morad Salhi:** Simulation, Writing - review & editing. **Othmane**
18 **Horma:** Laboratory tests, Sample preparation, Writing - review & editing. **Ahmed Mezrhab:**
19 Investigation, Writing - review & editing, Supervision. **Mustapha Karkri:** Software, Writing -
20 review & editing, Supervision. **Samir Amraqui:** Writing - review & editing.

1 Thermal and mechanical characterization of adobes bio-sourced with
2 *Pennisetum setaceum* fibers and an application for modern buildings

3 Mouatassim Charai^{1,2*}, Morad Salhi¹, Othmane Horma¹, Ahmed Mezrhab¹, Mustapha Karkri²,
4 Samir Amraqui¹

5 ¹ Mechanics and Energy Laboratory, Faculty of Sciences, Mohammed First University, 60000 Oujda, Morocco.

6 ² Université Paris- Est, CERTES, 61 Av. du Général de Gaulle, 94010 Créteil Cedex, France.

7 * Corresponding author: *charai.m@yahoo.com* ; *mouatassim.charai@u-pec.fr*

8 **Abstract:**

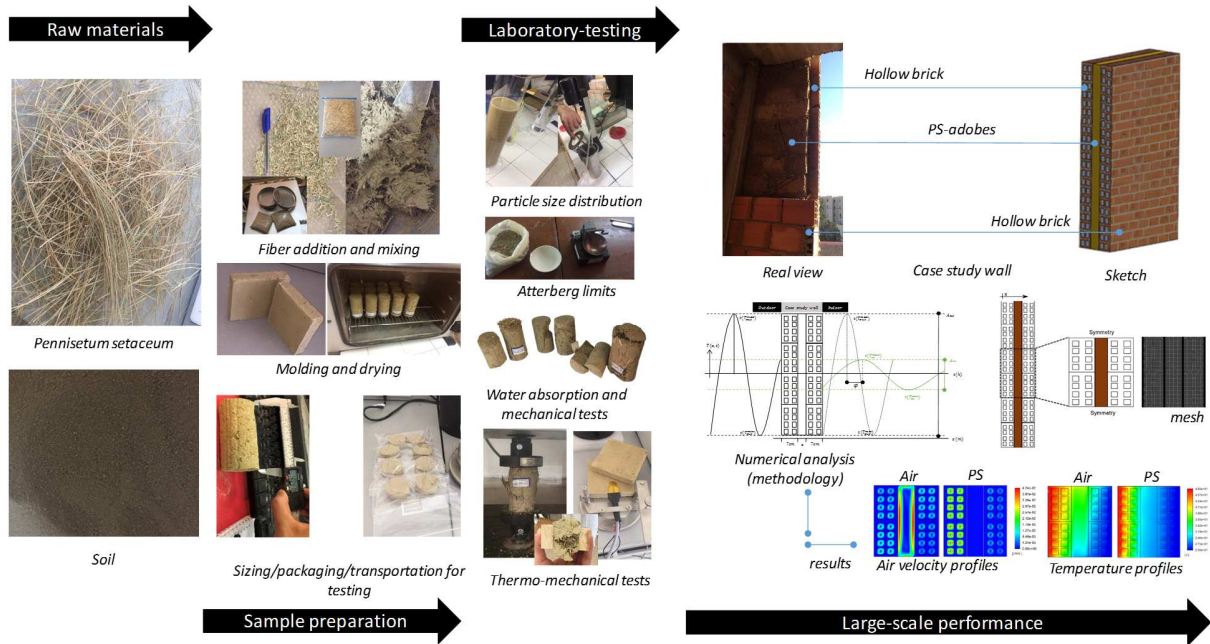
9 The purpose of this paper is twofold: to propose a sustainable eco-construction practice using
10 highly biosourced earth blocks in contemporary buildings, taking into account their poor
11 mechanical properties; and to assess the effect of incorporating *Pennisetum Setaceum* (PS) fibers
12 on the thermomechanical performance of adobes, where earth was biosourced with PS fibers at
13 weight percentages of 0, 2, 4, 6, and 8%. Firstly, raw materials' geotechnical, mineralogical,
14 chemical and microstructural characteristics were identified. Afterward, the thermal and
15 mechanical properties of produced PS-adobes were studied by hot disk method, uniaxial
16 compressive and tensile splitting strength tests. The impact of fiber content on the durability of
17 adobes was also discussed using capillary water absorption test. Experiments reveal that the
18 strength performance of adobes decreases with increasing fiber content while the cohesiveness of
19 mixtures improves. The cohesion improvement was confirmed via the water absorption test.
20 Adding 8%wt of PS fibers can improve the thermal insulation and the heat capacity of adobe by
21 56.7% and 17.9%, respectively. Laboratory testing was followed by CFD analysis to underline
22 the efficacy of a hybrid bio-based wall in which a PS-adobe layer is incorporated into a double
23 hollow brick wall. The numerical results show that a 10-h time lag was achieved with biosourced

1 earth layer thickness of 90 mm. As a result, high bio-content adobes may be employed as a green
2 thermal mass element in modern buildings with a contribution to thermal insulation.

3 **Keywords:**

4 Bio-sourced adobes; Hybrid bio-based wall; Sustainable buildings; Thermal inertia; Thermal
5 conductivity; Time lag.

1 Graphical abstract



2

1 **Highlights**

- 2 • Hybrid bio-based earth wall proposal for efficient and sustainable contemporary
3 buildings.
- 4 • Local adobes were manufactured using different Pennisetum Setaceum (PS) fiber
5 contents.
- 6 • Thermal, mechanical and durability performances of biosourced adobes are investigated.
- 7 • Wall's Time lag and decrement with different adobe layer thicknesses were identified.
- 8 • Eco-efficient wall with 10-h time lag was achieved for contemporary building design.

1 **Nomenclature**

2	α	thermal diffusivity ($\text{m}^2.\text{s}^{-1}$)
3	λ	thermal conductivity ($\text{W}.\text{m}^{-1}\text{K}^{-1}$)
4	ρ	density ($\text{kg}.\text{m}^{-3}$)
5	φ	time lag (h)
6	A	surface area (m^2)
7	C_b	absorption coefficient ($\text{g}.\text{cm}^{-2}.\text{min}^{-1/2}$)
8	c_p	specific heat capacity ($\text{J}.\text{kg}^{-1}.\text{K}^{-1}$)
9	D	sample diameter (m)
10	f	decrement factor (-)
11	f_c	compressive strength (MPa)
12	f_t	tensile splitting strength (MPa)
13	m	sample mass (kg)
14	%wt	percent by total weight (%)

15 **Index**

16	w	wet
17	d	dry
18	in	indoor
19	out	outdoor

20 **Acronym**

21	AMEE	Moroccan Agency for energy efficiency
22	PS	Pennisetum Setaceum
23	RTCM	Thermal regulation of Moroccan construction

1 **1 Introduction**

2 The use of natural additives from agriculture in clay-based building materials as promising
3 construction solution has attracted a great deal of interest in recent decades. Several by-products
4 [1, 2] have been tested to improve the thermal insulation of bricks [3], as well as to gradually
5 replace conventional building materials in order to reduce the high carbon footprint of buildings.
6 Indeed, the incorporation of such materials (vegetable fibers, etc.) adversely affects the
7 compressive strength properties of building masonry. However, the addition of a small amount of
8 short fibers can play the role of reinforcement and solve optimally this problem with a remarkable
9 gain in strength [4, 5].

10 Since raw earth is the most eco-friendly component traditionally used in brick making, the
11 combination of agro-additives with clay matrix can be considered as one of the great potential
12 practices for greening the building industry. This basic mixture motivates a number of researchers
13 to try developing smart lightweight building envelopes through benefiting from the high thermal
14 mass of clay and the powerful effect of agro-aggregates on the hygrothermal performance of
15 bricks [6].

16 Series of studies have been conducted on bio-sourced clay bricks by adding agro-waste fibres and
17 grass that represent abundant, natural and renewable resources. For instance, Chiang et al. [7]
18 developed a new lightweight clay-brick using a mixture of soil with different percentages of rice
19 husks. A recent study by Jové-Sandoval et al. [8] was carried out on the investigation of three
20 types of vegetable fibres in adobe bricks compared to wheat straw. The literature results showed
21 the effectiveness of agro-based fibres in controlling cracking during the drying process of unfired
22 bricks and optimizing their thermal transport properties. However, more research in this direction
23 is required, adopting new local additives to develop high-performance and cost-effective bricks.

1 More recently, Ba et al. [9] studied the effect of high fiber content of *Typha australis* fibers, of up
2 to 55%, on the thermomechanical performance of clay bricks. The results show that the thermal
3 conductivity of clay decreased from 1.03 W/mK to 0.146 W/mK using 55% of 1 cm length fibers.
4 Nevertheless, the fiber addition showed a negative effect on the mechanical properties of clay. To
5 overcome the low mechanical properties of biosourced earth, in this work, a new way of using
6 unfired clay bricks with high fiber content in the building envelope is presented.

7 Besides the enhancement of the thermal insulation of adobes, the integration of biosourced earth
8 masonry in the building envelope improves the indoor conditions of spaces [10-16]. For instance,
9 Medjelekh et al. [16] studied the effect of unfired clay brick walls on the performance of buildings
10 under different dynamic scenarios. The experimental results demonstrated the excellent
11 hygrothermal performance of earthen walls under humidity fluctuations. More recently, the
12 efficacy of earth walls, compared to fired brick walls, in improving the indoor comfort level of
13 buildings by the passive regulation the fluctuations of temperature and relative humidity is
14 demonstrated [13].

15 In Morocco, the eastern region constitutes the largest semi-arid area in the country covered by
16 different layers of grass and steppes, comprising more than 2 million hectares of Alfa, 200
17 thousand hectares of Gramineae and various plant species [17, 18]. Therefore, this region
18 represents a fruitful area for testing the maximum of agro-based additives in the design of new
19 site-specific bio-sourced building materials and stimulates the biosourced industry at the national
20 level.

21 On the use of *Pennisetum* species, there is no study available on *Pennisetum Setaceum* as a
22 construction material. The objective of this present paper, thus, is to characterize the
23 thermophysical properties of *Pennisetum*-clay unfired bricks (PS-adobes). The results of the

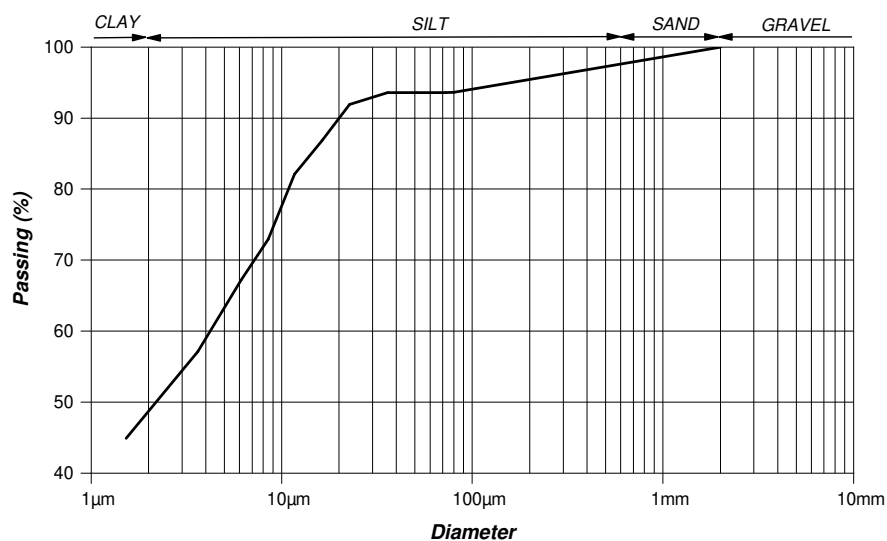
1 characterization will serve as input data to evaluate the feasibility and the energy performance of
2 PS-adobes as a new alternative material for the improvement of the energy efficiency of buildings
3 located in semi-arid climates.

4 **2 Raw materials and sample preparation**

5 **2.1 Soil**

6 2.1.1 Physical properties of soil

7 In order to improve local brick-making industry, the soil used in this study was extracted from
8 local quarries located in Twisent, eastern Morocco. This soil is also currently used by a local clay
9 hollow-brick factory (ARGILUX) located in Oujda. Grain size distribution by wet sieving and
10 sedimentation, as well as the Atterberg limits of the soil were identified according to NF EN ISO
11 17892-4 and NF P94-051, respectively [19, 20]. The particle size distribution, presented in Fig. 1,
12 showed that the soil used belonged to clayey soil, composed of 6.5 %wt sand, 45 %wt silt and
13 48.5 %wt clay (particle size < 2 μm). The Atterberg limits were: liquid limit ($w_L = 40\%$), plastic
14 limit ($w_p = 21\%$), and plasticity index ($PI = 19\%$).



15

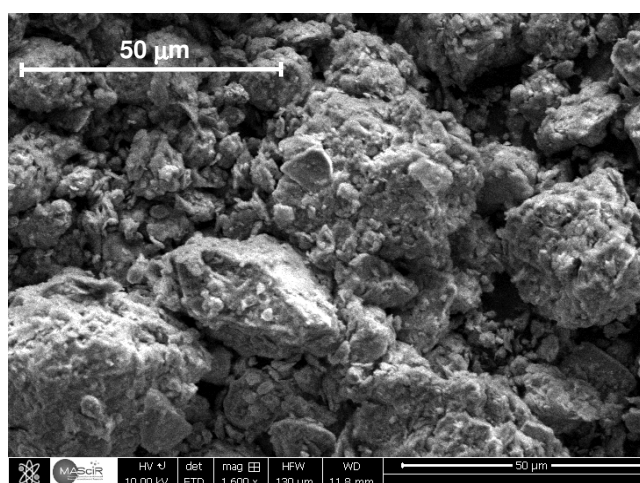
16

Fig. 1. Particle size distribution of soil.

1 2.1.2 Microscopic observations and chemical composition of soil

2 A detailed observation of the clayey soil was performed using field emission scanning electron
3 microscopy (FEI FEG 450 SEM) device. The microstructural morphology of the soil is given in
4 [Fig. 2](#). The SEM micrographs of soil clearly show the porous structure nature of soil, which is one
5 of the main characteristics resulting in the high sorption capacities and the low thermal
6 conductivity of unfired clay bricks compared to fired bricks, which are highly recommended in
7 the passive regulation of indoor humidity and temperature fluctuations. For further details on fired
8 and unfired clay bricks of the used soil, please refer to our previous comparative study in [\[21\]](#).

9 The SEM analysis was coupled with an energy-dispersive X-ray spectroscopy using EDS
10 BRUKER XFlash 6/30 apparatus to assess the main chemical compounds of the used soil. As
11 presented in spectrums of [Fig. 3](#), the main chemical elements of clay are Si, Fe and Al
12 respectively. EDS Results indicate that the soil is a non-calcareous clay with an average content
13 around 48.05 % of SiO₂, 19.78% of Al₂O₃ and 9.55% of Fe₂O₃. The used clay composed of a
14 significant amount of Bromine (Br). This is likely due to its incorporation into Al and Fe-
15 oxyhydroxides and the higher content of silicate minerals [\[22\]](#). The elementary chemical
16 composition is summarized in [Table 1](#).



17

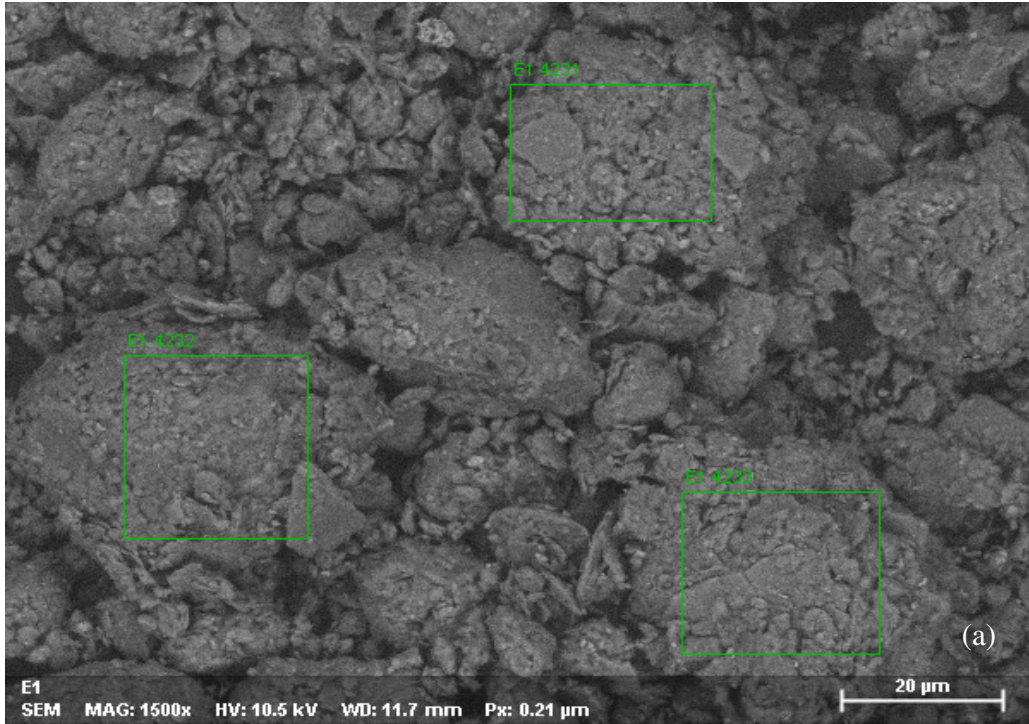
1 **Fig. 2.** SEM micrographs of soil.

2 2.1.3 Mineralogical characterization of soil

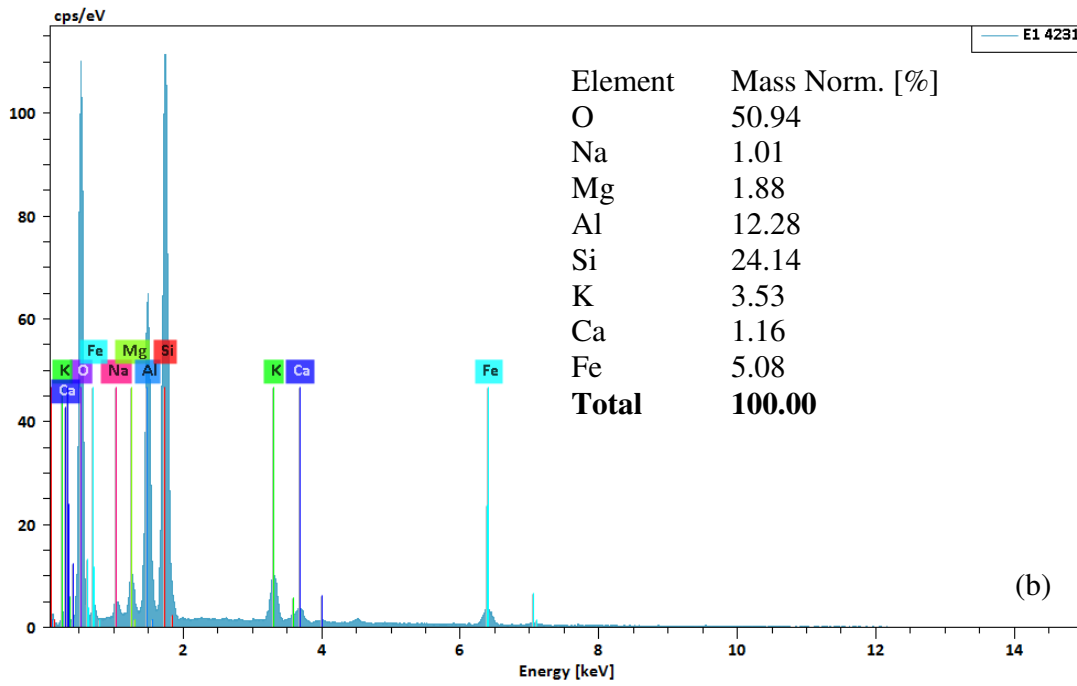
3 A complete semi-quantitative analysis of the clay was performed using an X-ray diffractometer
4 (Shimadzu XRD-6000, Cu-K α : 1.54060 Å) on both bulk and oriented samples. As expected, the
5 XRD pattern of bulk soil (Fig. 4a) shows the presence of quartz (SiO₂), kaolinite, illite, goethite
6 (Fe₂O₃, H₂O), and a small content of calcite (CaCO₃), plagioclase (CaAl₂Si₂O₈), siderite (FeCO₃)
7 and Rhodochrosite (MnCO₃). Note that the total clay represents all the clay minerals that exist in
8 the soil.

9 To identify minerals contained in our total clay, X-ray diffraction analysis on three oriented
10 samples was performed. Fig. 4b represents the XRD patterns of air-dried sample, sample heated
11 up to 500°C for two hours and sample exposed to ethylene glycol vapour until saturation. Finding
12 results show that the used soil is a mixed-layer Illite-Vermiculite with an important content of
13 Kaolinite.

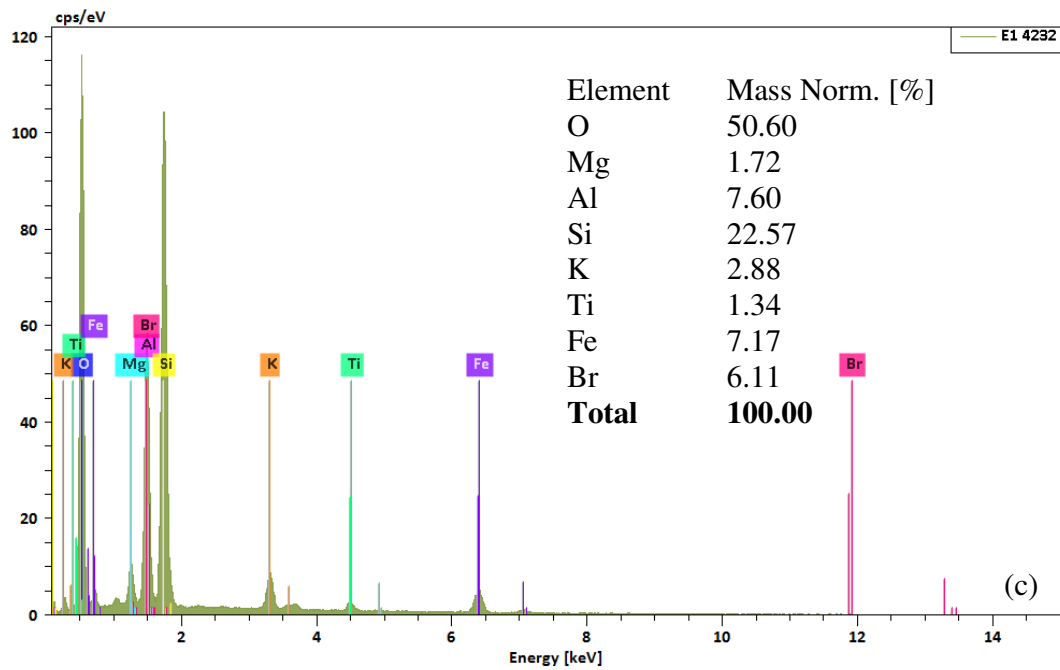
14 The thermal mineralogical behaviour of soil was assessed using a DTG-60 detector. The soil was
15 heated up to 1000 °C with a temperature rate of 20 °C/min in air atmosphere. TG-DTA curve of
16 used soil is presented in Fig. 5. The soil was subjected to a total mass loss of 9.39%. The curve
17 shows five main endothermic reactions, namely: evaporation of adsorbed water at 85 °C (1.87
18 %wt loss), dihydroxylation of goethite at 290 °C (0.71 %wt loss), dihydroxylation of clay
19 minerals, kaolinite [23], illite and quartz, at 516 °C and 670 °C (6.25 %wt loss) and
20 decarbonisation reaction due to calcite at 870 °C (0.56 %wt loss). All of the above soil analyses
21 are coherent and confirm each other.



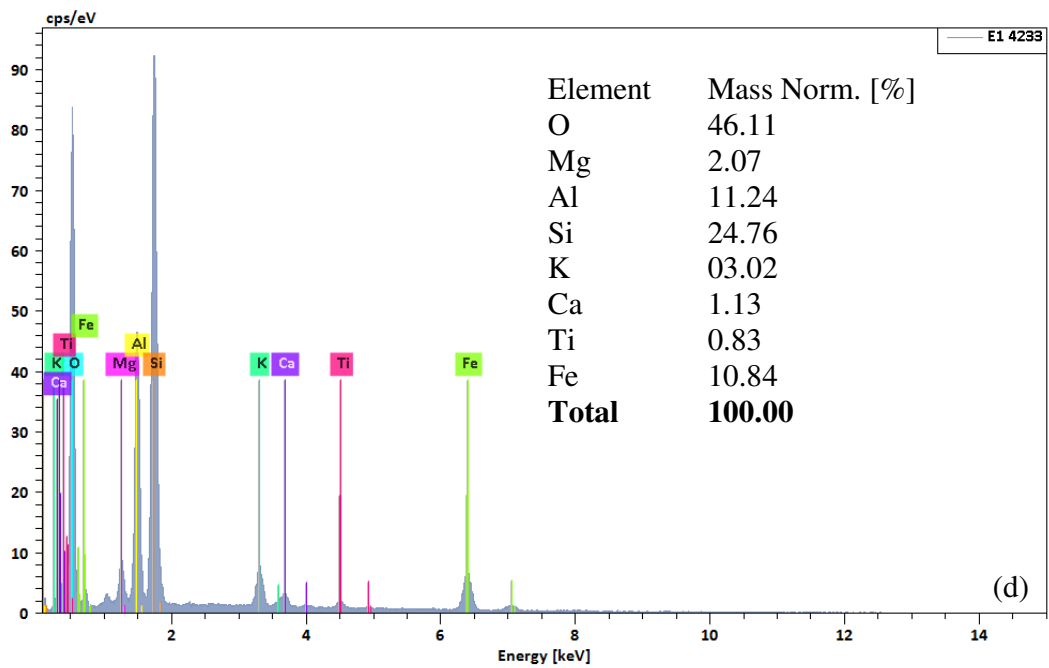
1



2



1



2

3

4

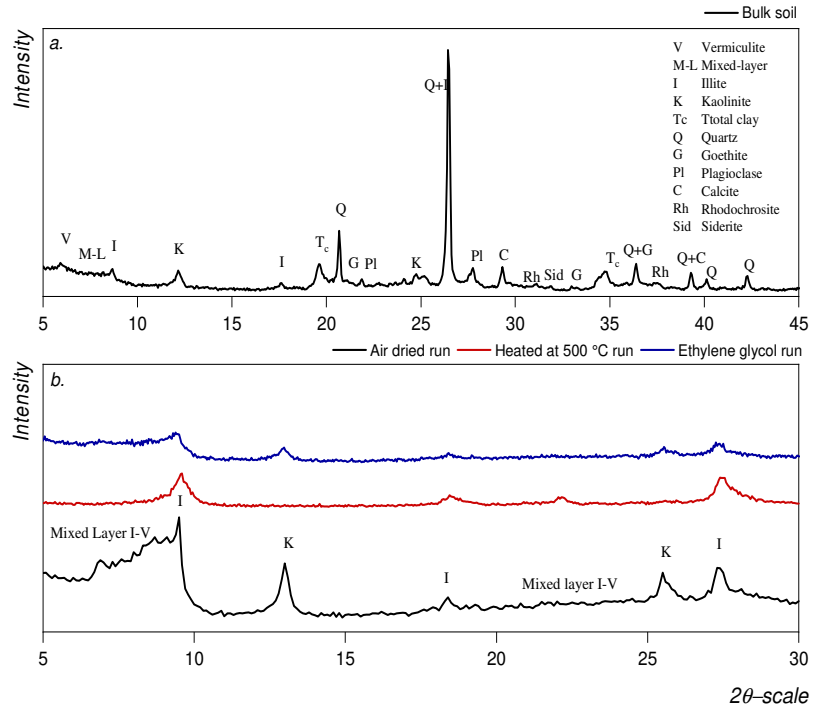
5

Fig. 3. SEM-EDS results of soil: (a) SEM image (b-d) EDS of three different spectra.

1

Table 1. Chemical composition of soil (%).

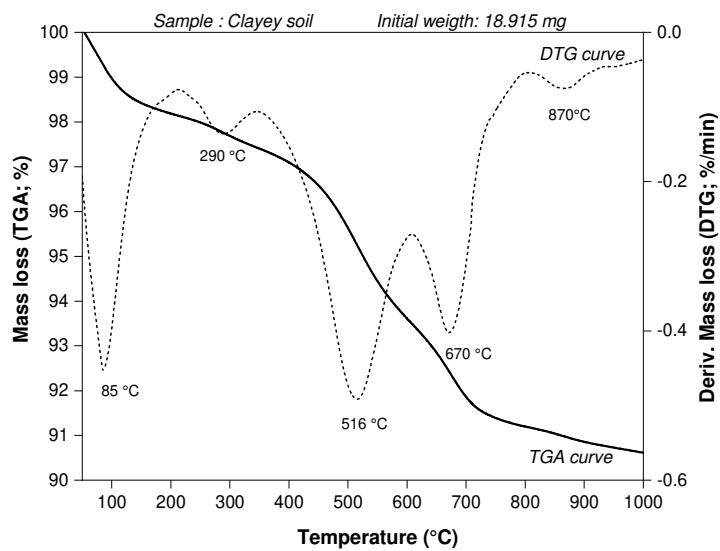
Oxides	SiO ₂	Al ₂ O ₃	Fe ₂ O ₃	Br	K ₂ O	MgO	Ti ₂ O	CaO	Na ₂ O
Value	48.05	19.78	9.55	5.70	3.39	2.90	1.69	1.49	1.27



2

3

Fig. 4. XRD patterns of soil: (a) bulk sample (b) oriented clay samples.



4

5

Fig. 5. TGA-DTG curve of soil

1 2.2 PS fibers

2 Due to their wide availability in eastern Morocco Region, Pennisetum Setaceum fibers were used,
3 in this study, as a partial replacement of clay to evaluate their potential for promoting the local
4 manufacturing of biosourced clay bricks. The fibers are cultivated and collected from the Faculty
5 of sciences of Oujda. Before evaluating the impact of Pennisetum Setaceum fibers on the
6 thermomechanical performance of produced PS-adobes, a literature investigation, X-ray
7 diffraction and a TGA analysis were performed on PS fibers.

8 Pennisetum Setaceum, also known as Fountain grass, is a warm-season ornamental grass widely
9 available in Middle East and North Africa (MENA) regions with semi-arid climate. Few studies
10 have been focused on Pennisetum Setaceum fibers. Yussof et al. [24] studied the tensile strength
11 of PS fibers as a function of time. This study showed that PS fibers have a maximum tensile
12 strength after three months of cultivation. Nkemka et al. [25]. The physicochemical properties of
13 PS fibers obtained from literature are summarized in Table 2.

14 **Table 2.** Physicochemical properties of PS fibers.

Property	Physical			Chemical		
	Grass length	Root diameter	Tensile force	Cellulose	Hemicellulose	Lignin
Unit	m	mm	N	%	%	%
Value	0.8 – 1.2	0.28-1.36	22	40.5 ± 0.3	29.4 ± 0.5	6.6 ± 0.7
Ref.	[26]	[24]	[24]	[25]	[25]	[25]

15

1 X-ray diffraction analysis was performed to evaluate the crystalline phase of PS fibers. The
2 diffraction pattern of PS fibers, presented in Fig. 6, indicates three main peaks at 2θ of 15.3, 22
3 and 37.65, corresponding to the principal cellulose signals of vegetable fibers [27]. The
4 crystallinity index is one of the main properties of cellulosic fibers, which can be empirically
5 calculated from the XRD spectrum as follows [28]:

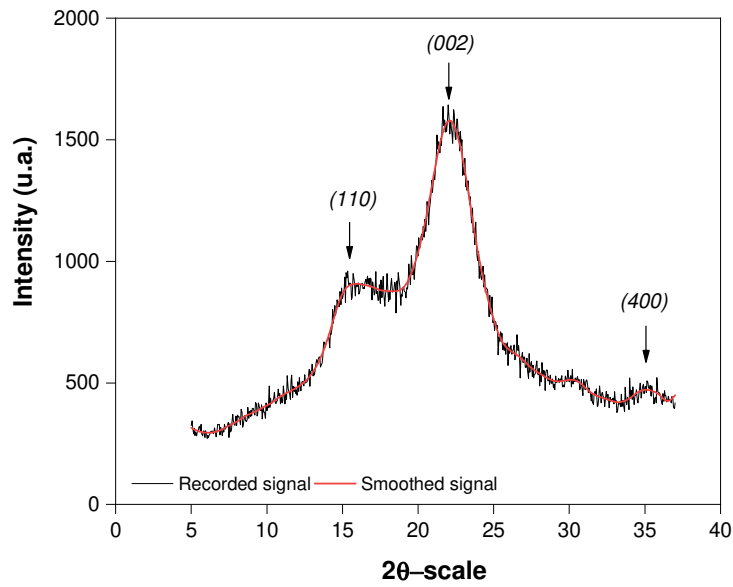
$$\text{CrI (\%)} = \frac{I_{002} - I_{\text{am}}}{I_{002}} \times 100 \quad (1)$$

6 Where I_{002} represents the intensity of the crystalline portion of cellulose corresponding to the
7 maximum intensity around 22° of 2θ -scale and I_{am} represents the amorphous portion of cellulose
8 corresponding to the minimum intensity between 18° and 19° of 2θ -scale.

9 On the basis of Fig. 6, the crystallinity index of PS fibers is found to be around 43%, compared to
10 hemp with CrI of 56% [29]. This result show that PS fibers composed of a high cellulose content,
11 which can be useful for the design of efficient building material units.

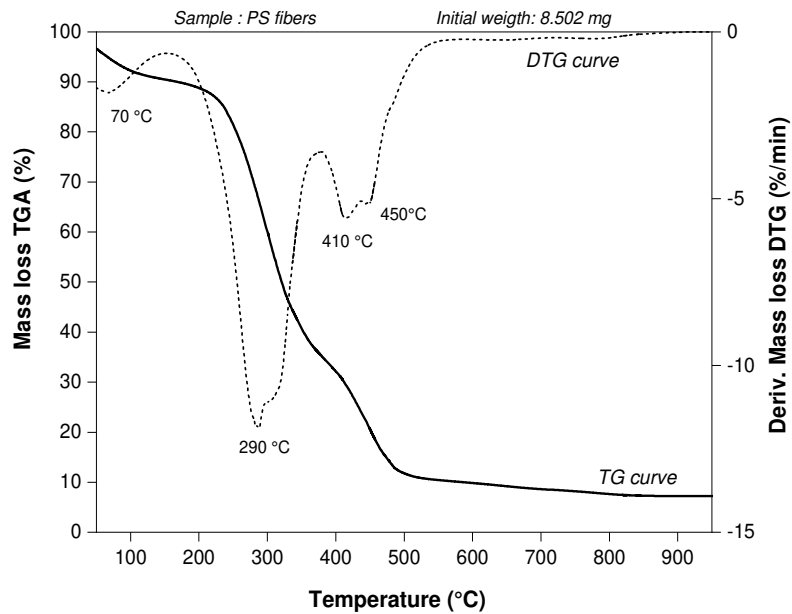
12 Also, the thermal gravimetric analysis was performed simultaneously on PS powder heated up to
13 1000°C at a constant temperature rate of $20^\circ\text{C}/\text{min}$ in air atmosphere. TG-DTG curve of PS fiber
14 is given in Fig. 7. The curve represents a typical thermal diagram of lingo-cellulosic substances.
15 After the hygroscopic water loss represented by the endothermic peak around 68°C , PS fiber was
16 subjected to three main exothermic reactions at 286, 450 and 800°C , respectively corresponding
17 to hemicellulose, cellulose and lignin decompositions [30]. Unlike the slow decomposition of
18 lignin with small mass loss at high temperature, TG-DTA curve of PS fiber shows a rapid
19 cellulose and hemicellulose decomposition with a significant mass loss of about 80%. The results
20 prove the presence of high amounts of cellulose in PS fibers, which can be effective in the
21 stabilization of unfired clay bricks.

1 Fig. 8 shows the microstructure of PS fibers. The porous structure of PS fibers is clearly observed
2 in the SEM image, which is an essential criterion for the improvement of the thermal insulation of
3 earth bricks.



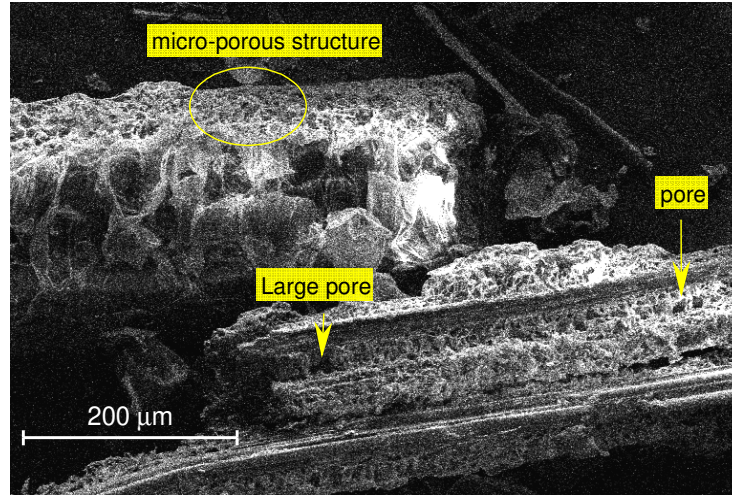
4
5

Fig. 6. XRD pattern of PS fibers.



6
7

Fig. 7. TGA-DTG pattern of PS fibers.



1

2

Fig. 8. SEM micrograph of PS fibers.

3 **2.3 Mix proportions and sample preparation of PS-adobes**

4 PS-adobes were prepared by manual dry mixing of the clayey soil (< 1 mm) with different weight
 5 percentage ratios of PS fibers of length 2 cm, for a given time until obtaining homogeneous
 6 mixtures. The details of the mix proportions are presented in [Table 3](#). For compaction, a same
 7 water-to-clay ratio (w/c) was then added to each mixture. As conducted by Ouedraogo et al. [\[31\]](#),
 8 the required water-to-clay ratio was calculated using [Eq. 2](#). Unlike the common studies on agro-
 9 based adobes [\[31-34\]](#), high fiber-to-clay ratios were considered in this paper (0, 2, 4, 6 and
 10 8%wt). The 8%wt was chosen as the maximum incorporation rate in order to ensure good
 11 compaction of the adobes produced. Beyond this value, compaction issues were observed during
 12 preparation. The reference case consisted of samples without PS fibers. The step-by-step PS-
 13 adobes preparation is illustrated in [Fig. 9](#).

$$(w/c)_{ratio} = \frac{w_L + w_P}{2} \quad (2)$$

14 In which w_L and w_P are respectively the calculated Atterberg liquidity and plasticity of the soil, in
 15 %. To success the laboratory-testing of samples, the wet mixtures were manually compacted in

1 three different kinds of moulds, as indicated in Fig. 10. Once the specimens were prepared and
 2 dried at the room temperature for 48 hours, they were placed in a drying oven at 60 °C until a
 3 constant mass was reached. Note that the tests were performed when the mass of the samples was
 4 stabilized.



5
6
7

Fig. 9. Sample preparation process.

Table 3. Mix compositions (% by total weight).

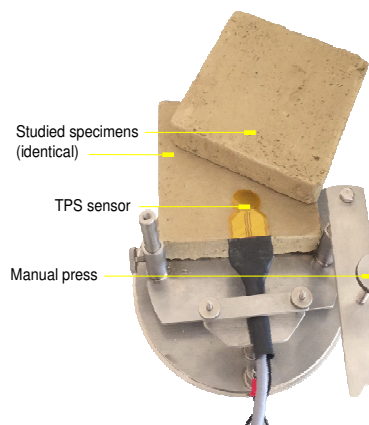
Mix code	Clay	PS fibers	(w/s) ratio
PS-adobe 0	100	0	Eq. 2
PS-adobe 2		2	
PS-adobe 4		4	
PS-adobe 6		6	
PS-adobe 8		8	

8 3 Methods

9 3.1 Hot disk method

10 Thermal conductivity, thermal diffusivity and volumetric heat capacity values of produced
 11 adobes were measured in accordance with ISO 22007-2 using the TPS 2200 (Hot Disk, Sweden)
 12 device [35]. Prior to tests, the sample-to-sensor contact surfaces were smoothed with a 400-grit

1 silicon carbide sandpaper to avoid any air-gap effect. Then, the measurements were conducted
2 by sandwiching a TPS double spiral Kapton sensor (ref. 5501) with a radius of 6.403 mm
3 between to identical specimens, as shown in Fig. 10. The TPS sensor was clamped between the
4 two specimens for a given time to ensure thermal stability using the manual press (Fig. 10), then
5 was heated by a constant electric power of 100 to 150 mW for 80 seconds. Thereafter, the
6 temperature increase of studied samples was monitored as a function of time by the same sensor.
7 Finally, the thermal transport properties were simultaneously estimated based on the recorded
8 time-dependent temperature increase using a hot disk analyser software v.7.0.0. Considering the
9 adobe heterogeneity, three measurements were performed at different positions for
10 parallelepiped samples (15x15x3 cm³), as in the work conducted by Madrid et al. [36]. For more
11 precision, the hot disk measurements were also conducted on three cylindrical samples 5 cm in
12 diameter and 2 cm in height per each mix. The test results are presented as the average value of
13 the measurements performed.



14

15

Fig. 10. Hot disk setup

16 **3.2 Water absorption test**

17 To evaluate the durability performance of produced adobes, the test of water absorption by
18 capillarity was carried out on three cylindrical specimens per adobe mix according to the French

1 standard XP-13-901 [37]. Considering the earth bricks-related worst case scenario, the test for
2 assessing the resistance of produced abodes to total water immersion was also performed on
3 three other cylindrical samples. Prior to tests, the specimens were oven-dried at 70°C for until
4 constant mass. The water absorption was presented by the capillarity water absorption
5 coefficient, C_b , which is expressed as follows:

$$C_b (\%) = \frac{m_w - m_d}{A \cdot \sqrt{t}} \quad (3)$$

6 In which m_d is the sample mass at dry state in kg, m_w is the sample mass after capillary
7 absorption for a duration t in kg, t is the test duration in min ($t=10$ min), A is the exposed surface
8 area in m^2 ($D=5$ cm).

9 **3.3 Mechanical tests**

10 The uniaxial compressive and tensile splitting strength tests were carried out using a
11 TESTWELL hydraulic press on cylindrical PS-adobe samples at the age of 28 days. Three
12 specimens per mix were tested each time. Prior to tests, the studied samples were oven-dried at
13 45 °C until a constant mass and then left for 2 hours at room temperature for stabilization.
14 According to the French standard XP P 13-901 [37], the constant mass is reached when the
15 difference between two daily successive weightings is less than 0.1%. By taking into
16 consideration the low mechanical properties of unfired clay bricks, both tests were run at a small
17 constant displacement rate of 0.01 $mm.s^{-1}$ [33]. As previously conducted by Jokhio et al. [38],
18 the tensile splitting and the compressive strength values are calculated using respectively the
19 following expressions:

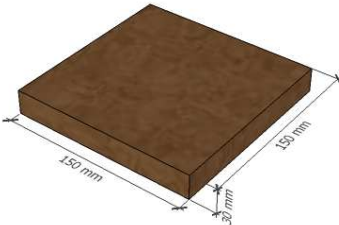
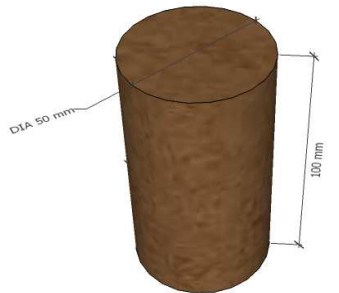
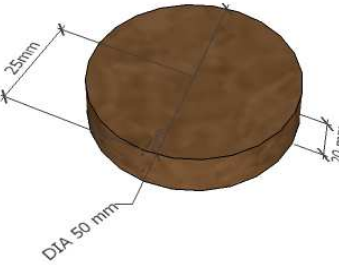
$$f_t = \frac{2F}{\pi DL} \quad (4)$$

$$f_c = \frac{4F}{\pi D^2} \quad (5)$$

1 In which f_t is the tensile splitting strength in MPa, f_c is the compressive strength in MPa, F is the
 2 maximum load applied in N, D is the diameter of the specimen in m², L is the length of the
 3 specimen (L=2D), in m.

4 To sum up, the overall laboratory tests are illustrated in [Table 4](#).

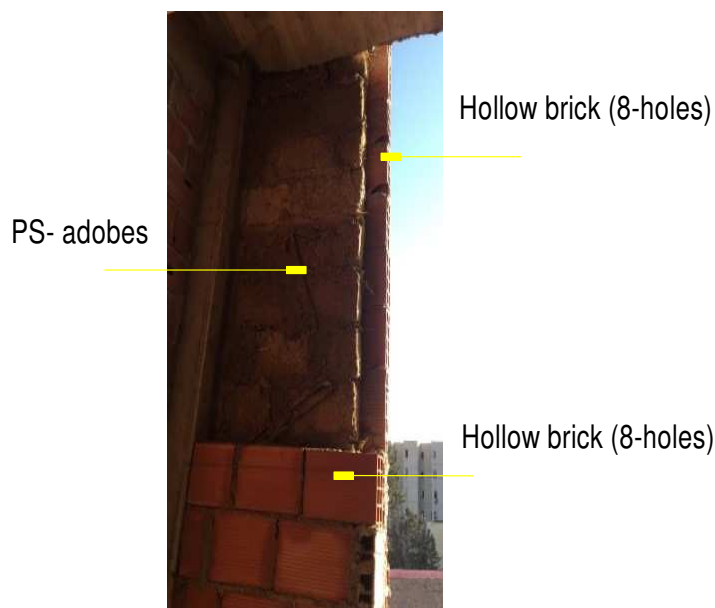
5 **Table 4.** Specimens' dimensions and tests considered in this work.

Sample	Dimension (mm)	Sample geometry	Experimental tests		
			Type	Units/mix/test	Standard
Slab	150×150×30		Bulk density	6	XP P 13-901 [37]
			Thermal test	6	ISO 22007-2: 2008 [35]
Cylinder	Dxe= 50×20		Uniaxial compressive test	3	XP P 13-901 [37]
			Tensile splitting test	3	EN 12390-6 [39]
			Capillary Water absorption test	3	XP P 13-901 [37]
			Total immersion water absorption test	3	NF P94-078 [40]
	Dxe= 50×100		Thermal test	6	ISO 22007-2: 2008 [35]

6

1 3.4 Thermal performance of a case study wall: hybrid bio-based wall

2 Following the experimental characterization of PS adobes, this section deals with the study of the
3 thermal behaviour of a hybrid bio-based wall (Fig. 11) integrating the developed earthen blocks
4 (PS-adobes 8) into a double hollow bricks wall using ANSYS-Fluent CFD code. The CFD
5 approach was adopted here in view of its excellent effectiveness in handling thermal problems,
6 particularly in the building field [41-44]. For better understanding, the effect of varying the
7 thickness of integrated biosourced earthen layer on the thermal performance of the proposed wall
8 was studied. The comparison between the performance of the green wall and typical Moroccan
9 walls corresponding to double hollow brick walls with air gap is also investigated.



10
11 **Fig. 11.** Hybrid bio-based wall.

12 3.4.1. Governing equations

13 Heat is transferred by natural convection through brick holes, and due to the small size of the
14 holes which results in a small temperature variation between their inner walls, the Boussinesq
15 approximation is considered for density [45], with the assumption that all other thermal transport

1 properties of air are constant. The construction materials and the thermophysical properties of
 2 each of the element of the green wall system are given in Table 5. For more precision, the
 3 characteristics of hollow bricks used are taken from the recent AMEE database on the main
 4 construction materials in Morocco [46], which corresponds to the 8-hole bricks manufactured in
 5 Eastern Morocco Region.

6 **Table 5.** Thermophysical properties of studied wall system.

Material	c_p (J.kg ⁻¹ .K ⁻¹)	λ (W.m ⁻¹ .K ⁻¹)	ρ (kg.m ⁻³)	Viscosity (kg.m ⁻¹ .s ⁻¹)
Brick ^a	729	0.203	990	-
PS adobes ^b	907	0.333	1303	-
Air ^c	1005	0.02462	1.177	1.983.10 ⁻⁵

7 ^a AMEE database [46].

8 ^b our work (see Table 7)

9 ^c Fluent library

10 The Navier-Stokes equations governing this system can be written as follows:

11 **Continuity equation**

$$\frac{\partial u}{\partial x} + \frac{\partial v}{\partial y} = 0 \quad (6)$$

12 **Momentum equation:**

$$\rho \left(\frac{\partial u}{\partial t} + \frac{\partial(uu)}{\partial x} + \frac{\partial(vu)}{\partial y} \right) = -\frac{\partial p}{\partial x} + \mu_t \left(\frac{\partial^2 u}{\partial x^2} + \frac{\partial^2 u}{\partial y^2} \right) \quad (7)$$

$$\rho \left(\frac{\partial v}{\partial t} + \frac{\partial(uv)}{\partial x} + \frac{\partial(vv)}{\partial y} \right) = -\frac{\partial p}{\partial y} + \mu_t \left(\frac{\partial^2 v}{\partial x^2} + \frac{\partial^2 v}{\partial y^2} \right) + \rho g \beta (T - T_0) \quad (8)$$

13 **Energy equation:**

$$\rho \left(\frac{\partial T}{\partial t} + \frac{\partial(uT)}{\partial x} + \frac{\partial(vT)}{\partial y} \right) = \left(\frac{\mu}{Pr} + \frac{\mu_t}{\sigma_t} \right) \left(\frac{\partial^2 T}{\partial x^2} + \frac{\partial^2 T}{\partial y^2} \right) \quad (9)$$

1 In the solid zones of the brick and the PS-adobe layer, heat transfer is done by conduction,
2 according to Eq. 10.

$$\rho c \frac{\partial T}{\partial t} = -\lambda \left(\frac{\partial^2 T}{\partial x^2} + \frac{\partial^2 T}{\partial y^2} \right) \quad (10)$$

3 3.4.2. Boundary conditions and Climate data

4 **Climate data.** To be more realistic and precise in our numerical analysis, either at the level of the
5 results obtained, or at the level of compatibility with the specific climatic conditions of eastern
6 Morocco where the proposed wall is built, we used real-time meteorological data obtained from
7 a high precision meteorological (HPM) station installed at Mohammed First University shown in
8 Fig. 12. In order to quantify the thermal performance of the proposed case study wall, a hot
9 summer day in July was selected to implement the input sol-air temperature, representing the
10 outside surface heat wave of the wall [47].



11

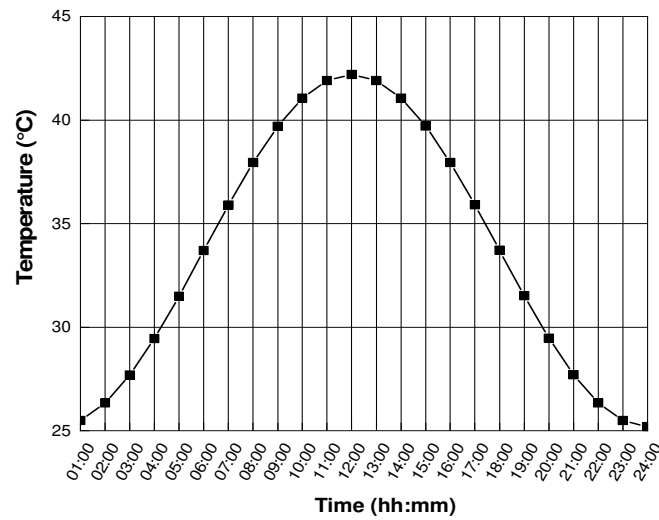
12

Fig. 12. Meteorological station used.

13 The variation of the sol-air temperature that characterizes the temperature of the outside heat
14 wave is illustrated in Fig.13. This heat wave is formed using a mathematical model that
15 approximates the real-time variation of the ambient temperature obtained from the selected day
16 during 24 h.

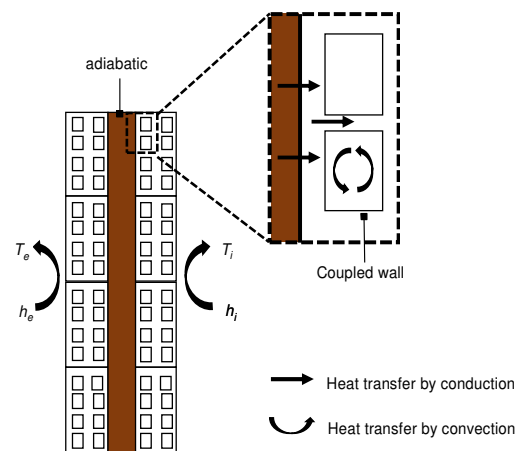
$$T_{sa}(t) = \overline{T_{amb}} + T_{max} \cos\left(\frac{\pi}{12}(t - 14)\right) \quad (11)$$

1 Here, T_{sa} is the temperature of the heat wave outside of the wall in question, $\overline{T_{sa}}$ and T_{max} are is
 2 the average temperature during a 24-h period and the maximum temperature of the outside
 3 temperature of the selected day respectively.



4
 5 **Fig. 13.** Hourly variation of the sol-air temperature.

6 **Boundary conditions.** Natural convection occurs on both the external and internal faces of the
 7 investigated wall, which depends on the external heat transfer coefficients. The thermal coupled
 8 condition and the non-slip momentum condition are applied to the concatenated solid-liquid and
 9 solid-solid zones. The boundary conditions are summarized in Fig. 14 and Table 6.



10

1 **Fig. 14.** Schematic diagram of the boundary conditions in the case study wall.

2 **Table 6.** Used boundary conditions.

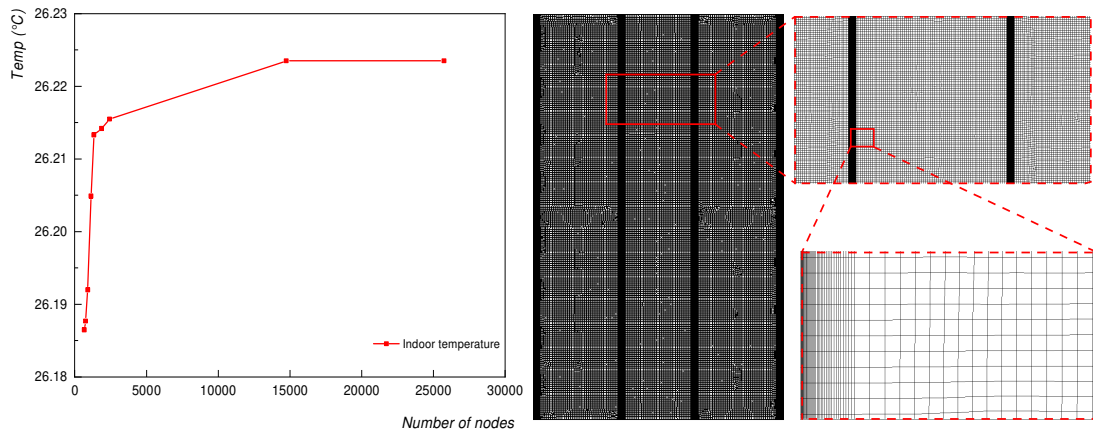
Zones	Conditions
External face	$-k_b \frac{dT}{dn} = h_e(t)(T_b - T_{amb})$
Infernal face	$-k_b \frac{dT}{dn} = h_i(t)(T_b - T_{amb})$
Horizontal Interface of the hole	$k_b \frac{dT}{dy} = k_f \frac{dT}{dy}$
Horizontal Interface of the hole	$k_b \frac{dT}{dx} = k_f \frac{dT}{dx}$
Solid/fluid walls	No slip velocity

3 3.4.3. Numerical procedure

4 **Used method.** A 2D steady-state simulation was performed using the CFD method. In this
5 method, the system of equations is solved by the finite volume method. The PISO algorithm and
6 the standard scheme were used to solve the velocity-pressure coupling and compute the pressure,
7 respectively. The convergence criterion was set at less than 10^{-6} .

8 **Mesh independence test.** In our study, a 2D structured quadrilateral grids is used in the
9 computational domain (Fig. 15), with refined grids near the air-solid and solid-solid regions to
10 increase the precision where the variation of thermal and dynamic phenomena is more important.
11 This technique is used in most CFD studies [48, 49]. This step has been carried out to optimize
12 and achieve the independency of the obtained results with respect to the mesh. The average
13 temperature at the level of the internal wall has been estimated for different mesh cell sizes, as
14 presented in Fig. 15. The results reveal that when the grid mesh is increased, the average
15 temperature of the interior wall rises; nonetheless, the temperature does not vary from 15000

1 total cells, and it is almost the same for 27000 cells. As a result, a mesh with a total number of
2 15000 was chosen to reduce computation time on one hand, while providing an accurate
3 prediction of the results.



4

5

Fig. 15. Mesh independence test and the grid system of the studied wall.

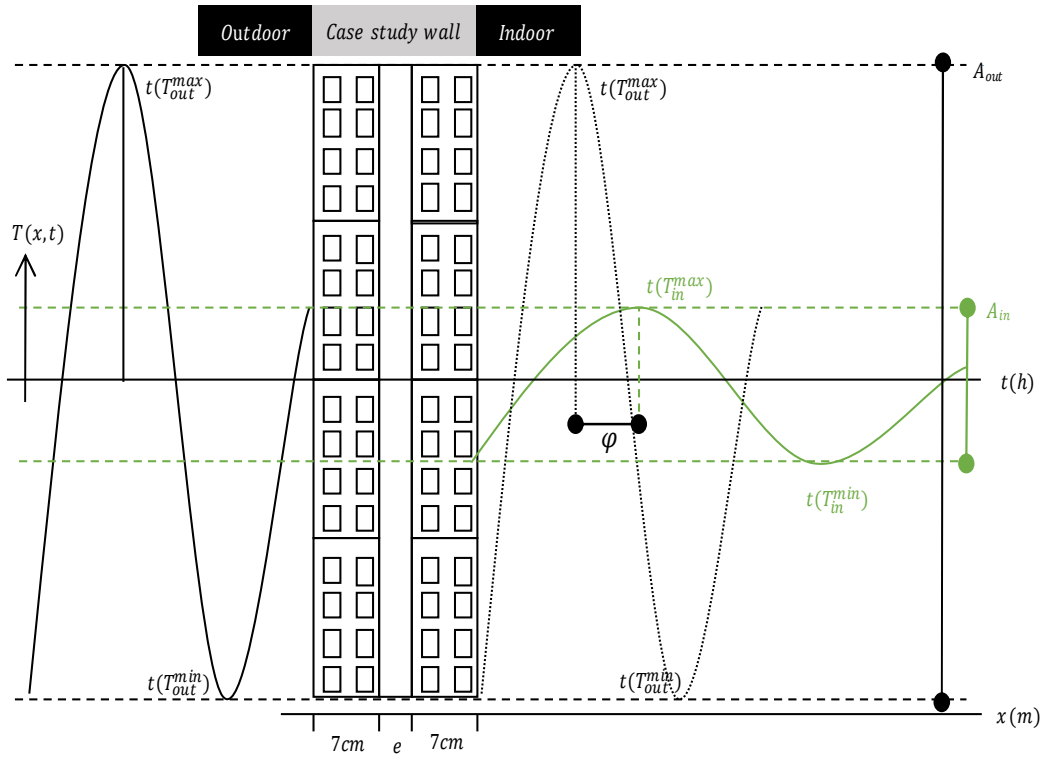
6 **Outputs.** The thermal performance of the proposed wall system is evaluated by the calculation of
7 the time lag and decrement factors. Indeed, during the propagation of outside heat waves through
8 the external surface of the wall, it takes a certain time before it reaches the inner surface. This
9 time interval is identified by the time lag, which characterizes the time interval between
10 temperature maximums at the outside and the inside of the wall in question when subjected to a
11 periodic heat wave called soil-air temperature [47]. Besides, the decrement factor presents the
12 ratio of the amplitude of the heat wave between the outer and inner wall. Both of these factors
13 are commonly used of the characterization of the thermal performance of walls [47, 50]. It
14 should be noted that large time lags and low decrement factors are essential to ensure excellent
15 thermal comfort levels and decrease the space heating and cooling demand of buildings. Fig.
16 16 shows a simplified scheme of the time lag (φ) and the decrement factors (f). As seen in Fig.
17 16, the time lag and the decrement factors are expressed respectively as follows [47]:

$$\varphi = \begin{cases} t_{T_{in}^{max}} - t_{T_{out}^{max}} & \text{when: } t_{T_{in}^{max}} > t_{T_{out}^{max}} \\ t_{T_{in}^{max}} - t_{T_{out}^{max}} + P & \text{when: } t_{T_{in}^{max}} < t_{T_{out}^{max}} \end{cases} \quad (12)$$

$$f = \frac{A_{in}}{A_{out}} = \frac{T_{in}^{max} - T_{in}^{min}}{T_{out}^{max} - T_{out}^{min}} \quad (13)$$

1 Here, φ is time lag of the studied wall, f is the decrement factor, $t_{T_{in}^{max}}$ and $t_{T_{out}^{max}}$ represent
 2 respectively the times when indoor and outdoor temperatures reached the maximum, A_{in} is the
 3 amplitude of indoor temperature profile, A_{out} is the amplitude of outdoor temperature profile. P
 4 is the heat wave period, which is defined to be equal to:

$$P = 24(\text{hours}) \times 60(\text{mins}) \times 60(\text{sec}) = 8760 \text{ sec} \quad (14)$$



5
6 **Fig. 16.** The schematic of temperature time lag φ and decrement factor f .

7 **4 Results**

8 **4.1 Thermophysical properties of PS-adobes**

1 The average values of the thermophysical properties obtained for each PS-adobe mix are listed in
2 [Table 7](#).

3 As expected, the bulk density decreased with increasing PS fiber contents. This decrease can be
4 explained by the creation of porosity in the clayey matrix, which is the main property for
5 improving the thermal insulation of biosourced adobes. For this reason, the reduction of the
6 thermal conductivity with the incorporation of PS fibers is observed. The results show that an
7 improvement of the thermal insulation of up to 56.7% can be achieved by the addition of 8% in
8 weight of PS fibers to clay, representing a decrease from $0.770 \text{ W.m}^{-1}.\text{K}^{-1}$ to $0.333 \text{ W.m}^{-1}.\text{K}^{-1}$.
9 There again, for the thermal diffusivity, PS-adobes with 8%wt of PS fibers exhibit the lowest
10 thermal diffusivity value of $0.282 \text{ mm}^2.\text{s}^{-1}$, which is a percentage enhancement of 45.8%
11 compared to clay alone.

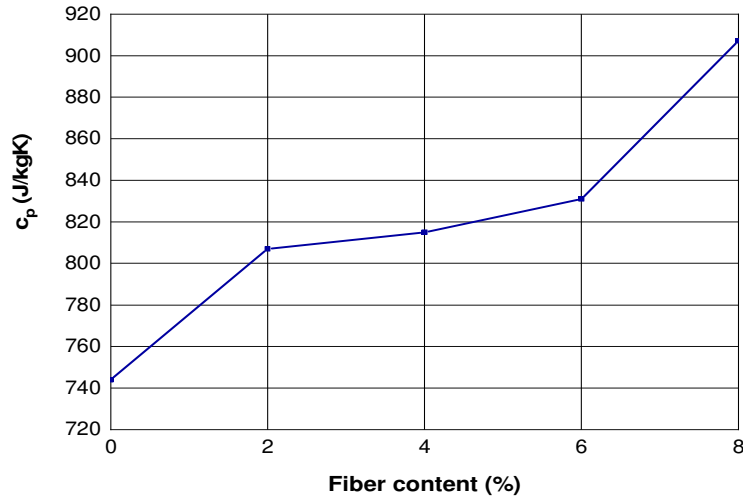
12 Another important property is the heat storage capacity of the PS-adobes, which is essential for
13 discussing the thermal performance of building materials. This property is simply deduced from
14 the division of the volumetric heat capacity obtained by the hot disk method by the density. The
15 heat capacity of produced PS-adobes is given in [Fig. 17](#). As can be seen, the incorporation of 8%
16 in weight of the PS fibers improves the heat storage capacity of adobes from $744 \text{ J.kg}^{-1}.\text{K}^{-1}$ to 907
17 $\text{J.kg}^{-1}.\text{K}^{-1}$.

18 Based on these results, we can affirm the efficiency of the use of PS fibers for the manufacture of
19 lightweight and thermal insulating adobes with enhanced thermal inertia.

20 **Table 7.** Thermophysical properties of PS-adobes.

Fiber content (%)	ρ (kg.m^{-3})	λ ($\text{W.m}^{-1}.\text{K}^{-1}$)	α ($\text{mm}^2.\text{s}^{-1}$)	ρc_p ($\text{MJ.m}^{-3}.\text{K}^{-1}$)
0	1985 ± 86	0.770 ± 0.001	0.521 ± 0.004	1.479 ± 0.009
2	1806 ± 34	0.558 ± 0.003	0.382 ± 0.012	1.458 ± 0.037

4	1787±39	0.460±0.001	0.316±0.003	1.457±0.013
6	1412±19	0.358±0.001	0.305±0.002	1.174±0.006
8	1303±15	0.333±0.002	0.282±0.006	1.182±0.009



1

2

Fig. 17. Specific heat capacity versus fiber content of PS adobes.

3 **4.2 Water absorption of PS-adobes**

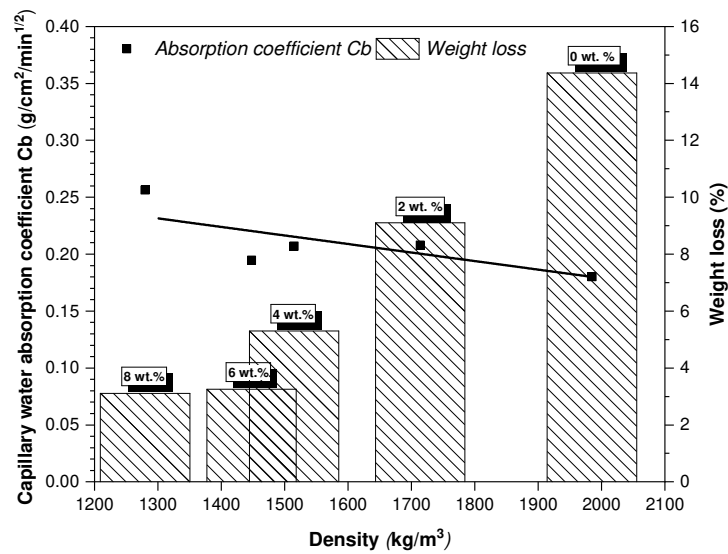
4 The first observation after total immersion of cylindrical PS-adobes in water is that biosourced
5 adobes did not resist full immersion (Fig. 18), as previously discussed by Achenza et al. [51]. For
6 this reason, when using clay for construction, additional measures must be considered to
7 waterproof the earth building envelope.

8 Fig. 18 illustrates the results of the water capillary test performed on cylindrical PS-adobes. Two
9 distinct things can be seen in the figure. First, the increase in fiber content increases the water
10 absorption of adobes, which is expected due to the hydrophilic nature of plant fibers. Also the
11 formation of voids in such biosourced composites is another reason for the high-water uptake.
12 On the other hand, the weight loss after water absorption test was also presented in Fig. 19 to
13 evaluate the effect of PS fiber content on the durability of adobes under wet conditions. The
14 results clearly show that the addition of PS fibers improves the resistance of adobes to water

1 capillarity, as evidenced by the decrease in the decomposition of mixtures shown in Fig. 20. This
 2 is attributed to the excellent adherence of plant fibers to the clayey matrix. The finding agrees
 3 well with the results reported by Ouedraogo et al. [31] and Danso et al. [52] and who
 4 demonstrated the effectiveness of fiber addition in the durability of adobes due to the high
 5 adhesion of biosourced clay mixtures compared to clay alone.



6
 7 **Fig. 18.** Water absorption test by total immersion of PS-adobes (Top View).



8
 9 **Fig. 19.** Capillary water absorption of PS-adobes.

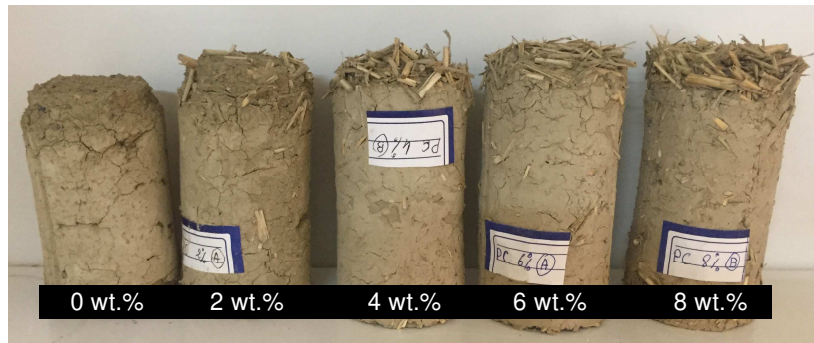


Fig. 20. PS-Adobes after capillarity water absorption test.

4.3 Mechanical behaviour of PS-adobes

The compressive (Fig. 21) and the tensile splitting (Fig. 22) strengths of the PS-adobes are presented in Fig. 23.

The increasing PS fiber contents lead to a decrease in the mechanical properties of the adobe.

The addition of 2%wt of PS fibers shows a drastically reduction of the compression and tensile splitting strengths of up to 40% and 67%, respectively. Above 2%wt of addition, a slight

decrease between 55-59% and 70-73% was observed, respectively for the compressive and the tensile splitting strengths. This significant decrease was expected due to the high fiber content

adopted in this study. Similar observations were found in the study conducted by Khoudja et al. [53] on the effect of date palm fibers between 0 to 10%wt on the thermomechanical properties of earth blocks.

Despite the poor mechanical properties obtained, an interesting observation was that the higher the addition of PS fibers, the better the cohesion of adobes. This can be clearly seen in Fig. 24a

and Fig. 24b, where the adobes containing PS fibers are still consistent after mechanical testing, compared to clay alone. Fig. 24c shows the overall comparison between adobes without and with

8%wt of PS fibers after water absorption and mechanical testing. Based on the figure, we can confirm the effectiveness of PS fibers on the cohesion of adobes under harsh conditions, which

1 could be useful for improving the earthquake resistance of adobe structures. Further building-
2 scale studies are needed to discuss this point.

3

4

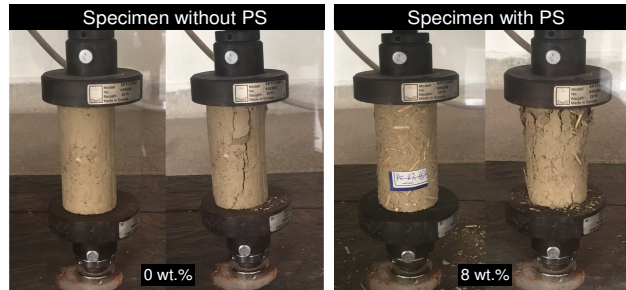


Fig. 21. Compressive strength tests.

5

6

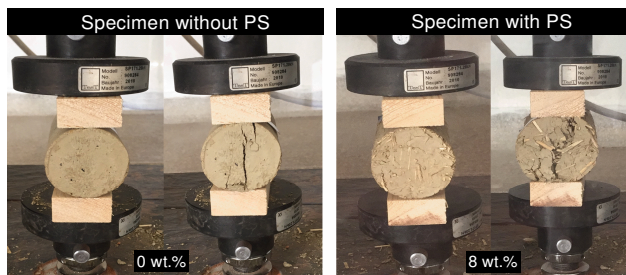


Fig. 22. Tensile splitting strength tests.

7

8

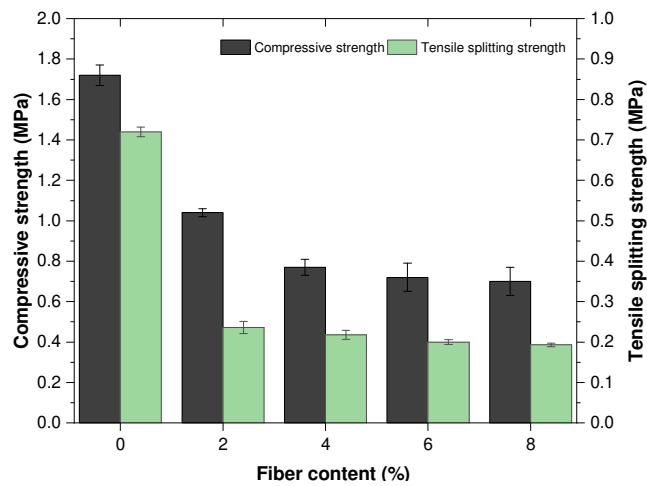


Fig. 23. Mechanical strength of PS-adobes specimens.

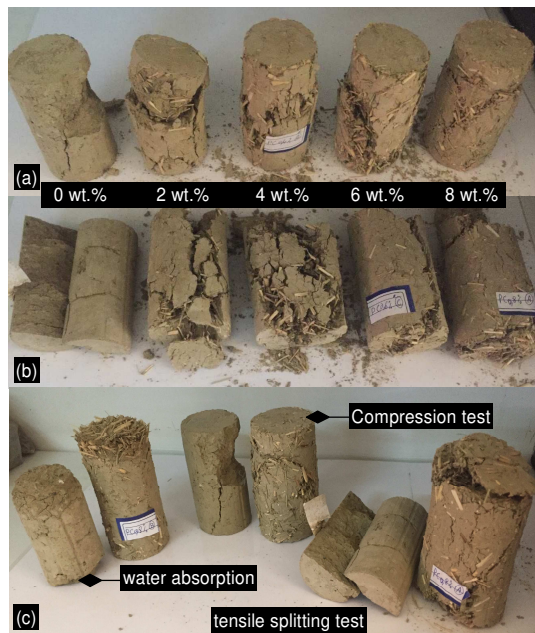


Fig. 24. PS-adobes after laboratory tests (0%wt vs. 8%wt).

4.4 Correlation between density and thermomechanical properties

It is worth investigating the possible relationship between thermomechanical and density properties of the developed biosourced adobes for the identification of optimum mixtures.

Despite the lack of knowledge about the relationship between compressive strength and density of biosourced adobes, several studies conducted on bio-based earth bricks [50, 53, 54] have reported two acceptable patterns, describing the decrease in thermal conductivity that generally follows a parabolic or linear regression as density decreases.

Fig. 25 gives the compressive strength and thermal conductivity of produced PS-adobes versus density at dry state.

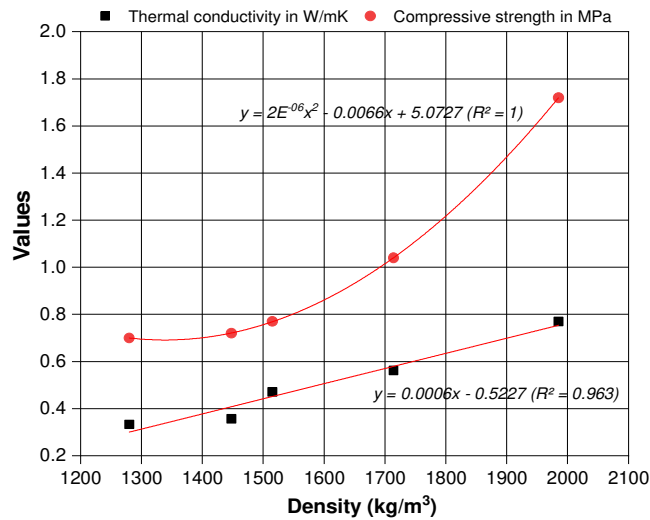


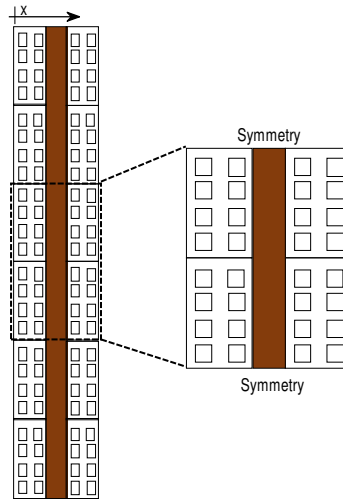
Fig. 25. Thermomechanical properties versus density.

1
2
3 A strong polynomial relationship between compressive strength and density is clearly observed,
4 with perfect correlation ($R^2=1$). The good linear correlation between thermal conductivity and
5 density of PS-adobes is also observed ($R^2>0.96$). These results are in line with literature
6 confirming the poor mechanical strength of adobes containing high amount of vegetable fibers
7 due to its negative effect on the cohesion of the clay matrix. For this reason, research conducted
8 on structural earth blocks focus on stabilizing adobes by low-fiber content addition or high
9 compaction techniques. Nevertheless, using a high fiber content ratio improves the thermal
10 insulation of adobes while also boosting their thermal heat capacity. The next section examines
11 the use of a novel construction method of using high-biosourced adobes in the building envelope,
12 taking into account the poor mechanical strength of earth.

13 **4.5 Thermal performance of hybrid bio-based wall**

14 In this section, the performance of the proposed hybrid wall is discussed. Note that the thickness
15 of each hollow brick is 7 cm. In order to evaluate the influence of the developed PS-adobes on
16 the thermal behaviour and heat transfer of the wall, a PS-adobe layer thickness ranging from 1 to
17 9 cm is considered.

1 Due to the symmetry of our system, and in order to reduce the computational time, we did not
2 simulate the system with the real dimensions of the wall, but rather with a part of the wall made
3 up of two blocks, as indicated in Fig. 26. To this end, the symmetry condition was applied at the
4 top and at the bottom of the chosen part of the wall.



5

6

Fig. 26. Schematic model of the case study wall.

7 As a first step, we specified the thickness of a 8%wt PS-adobe layer at 5 cm and we studied two

8 different cases, the case where the space between two bricks is filled with air (typical wall), and

9 the case where the PS-adobe layer is incorporated between the two hollow bricks (hybrid bio-

10 based wall). Fig. 27 shows the air velocity profile for both cases at 13h. In the case of

11 brick/air/brick, a high airflow circulation was observed inside the air gap due to natural

12 convection. Regarding the holes of the bricks, the air velocity is almost the same in all the holes.

13 While where the air gap is replaced by the PS-adobe layer, the air velocity is higher in the

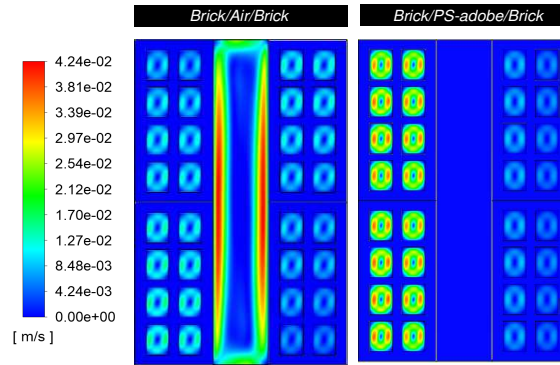
14 perforations of the first brick than in the second one. This dynamic behaviour is explained from a

15 thermal standpoint because the use of PS-adobe between the hollow bricks blocks the heat

16 propagation towards the second brick due to its low thermal conductivity, resulting in an increase

17 in natural convection in the first brick's holes. This finding supports the idea that incorporating

1 biosourced earth layer into conventional walls can act as a supplementary insulation element for
2 the building envelope, which could be a potential strategy for increasing the thermal comfort of
3 modern buildings.



4

5 **Fig. 27.** Air velocity distribution inside the case study walls (at 13h).

6 In what follows, we are more interested in the thermal aspect than in the dynamic aspect by
7 tracking the heat propagation as a function of time for the two scenarios studied.

8 [Fig. 28](#) depicts the fluctuation of the average surface temperature at the inner face of the studied

9 walls, as well as the change of the outdoor surface temperature excitation over time. Results

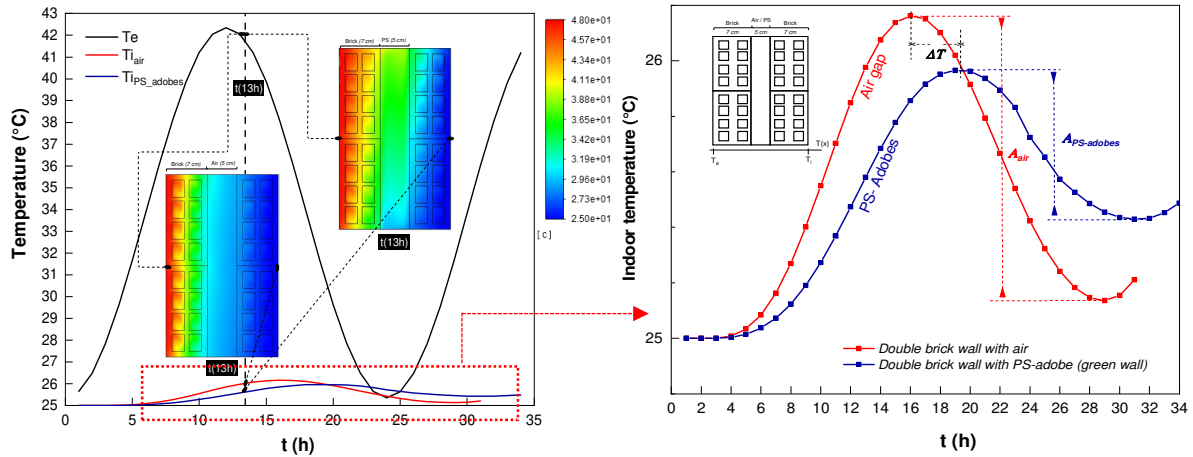
10 clearly demonstrate the good performance of studied walls in reducing the large amplitude of

11 outdoor heat waves, implying both configurations have a good decrement factor. However, the

12 hybrid bio-based wall presents the best configuration with a decrement factor roughly 0.03,

13 which means reducing outside temperature changes by twice as much as the typical

14 wall ($f=0.06$).



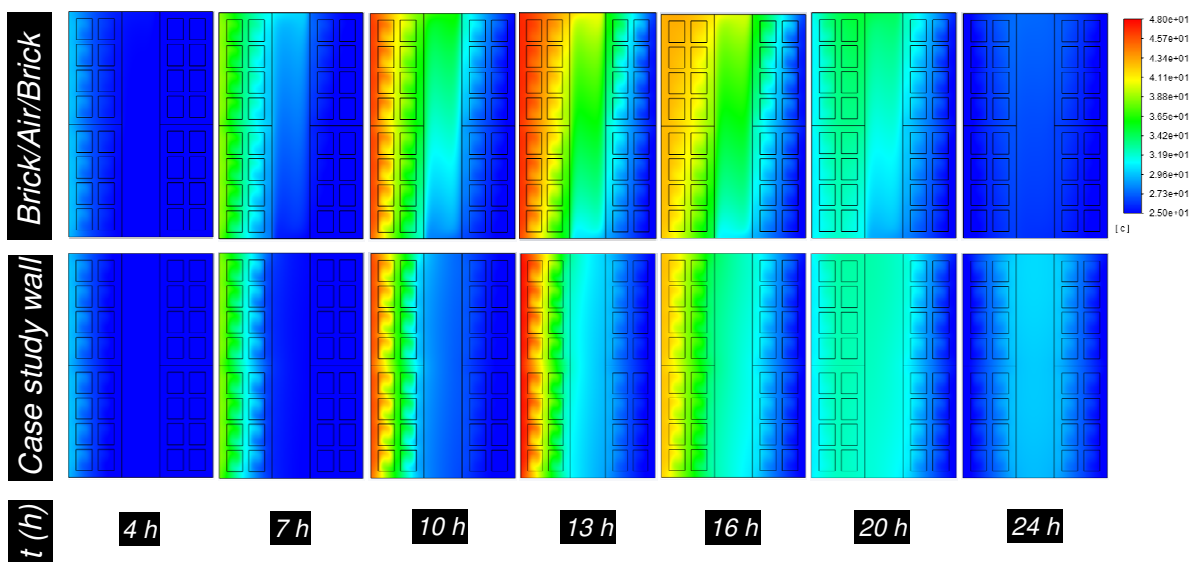
1
 2 **Fig. 28.** The average temperature on the exterior and interior faces of the wall along the day for
 3 different cases: brick/air/brick - brick/PS Adobes/brick.

4 It is also found that the maximum indoor surface temperature of the typical wall is approximately
 5 reached at 16h, whereas, for the hybrid wall, the maximum is attained at 19h. This indicates that
 6 the incorporation of PS-adobes can considerably improve the time lag of walls and thus insure a
 7 better occupant satisfaction in buildings. This time shifting improvement of about 3h is explained
 8 by the high thermal mass and the low thermal diffusivity and conductivity values of produced
 9 8%wt PS-adobes (Table 7).

10 The efficacy of biosourced adobe inclusion in modern building envelopes is clearly shown in
 11 Fig. 29 where the temperature distribution of brick/air gap/brick and brick/PS-Adobe/brick is
 12 presented for different times of the day.

13 In the first hours of the day the heat is propagated from the outside to the first brick. As time
 14 passes, the heat goes out from the first brick to the second brick. In the case of air gap
 15 configuration, the propagation is more remarkable compared to PS-adobe case because of the
 16 high thermal resistance of the latter. As indicated in the profiles depicted at 10h, this intriguing
 17 characteristic of the biosourced earth layer has led to a blockage of heat signal transmission to
 18 the indoor environment, which can be helpful in reducing overheating risk during summer

1 periods. After 16 hours, when the outside temperature starts to drop, the heat propagation also
 2 takes the opposite direction. More importantly, at 24h, it was found that the wall containing the
 3 PS-Adobe layer stores heat during the night hours due to this thermal inertia, which is an
 4 excellent property for the indoor temperature regulation, especially in summer [55, 56].
 5 From these findings, two conclusions can be drawn: the incorporation of agro-earthen layer into
 6 the building envelope can serve as both an auxiliary thermal insulation component for passive
 7 heating and thermal massing element for passive cooling, which appear to be beneficial
 8 regarding the enhancement of indoor thermal comfort level and reducing the annual energy
 9 demand [57].



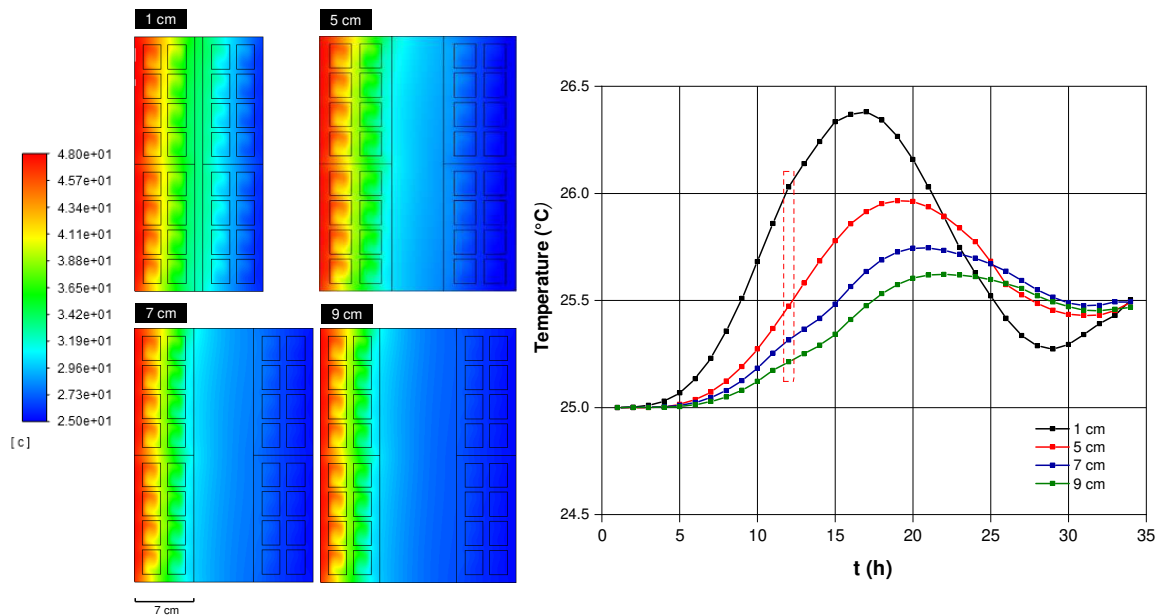
10

11 **Fig. 29.** Temperature distribution in the two systems brick/air/brick and brick/PS Adobes/brick
 12 for different times during the day.

13 In order to evaluate the effect of the thickness of the incorporated PS-adobe layer on the thermal
 14 behaviour in the hybrid wall assembly, four different thicknesses were studied: 1, 5, 7 and 9 cm.
 15 A maximum thickness of 9 cm was considered in this investigation due to the fact that the real
 16 case study wall (Fig. 11) is made up of 9-cm-thick adobe layer.

1 Fig. 30 shows the average temperature variation at the inner face of the studied wall during the
2 day for different thicknesses. The temperature distribution profiles at 13h of each of the cases are
3 also presented.

4 As expected, the results also show that the amplitude of the temperature fluctuation decreases
5 with the increase of PS-adobe layer thickness. For instance, at 13h, the temperature of the inner
6 surface of the wall with 1 cm tick adobe layer achieved 26.1°C, whereas, the addition of 9 cm
7 thick layer has led to a reduction of the temperature to 25.4°C. On the other hand, with the
8 increase of the thickness, the temperature curve loses gradually its wave form, highlighting the
9 potential use of hybrid walls in moderating the indoor temperature fluctuations in buildings.



10

11

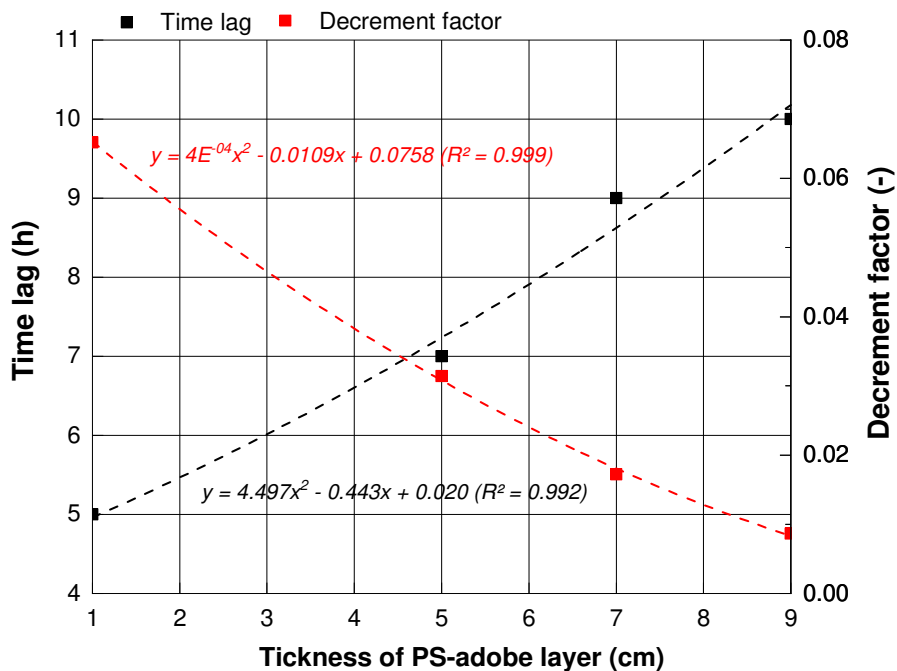
Fig. 30. Temperature distribution versus earthen block thickness.

12 The thermal performance of investigated wall as a function of the thickness of 8%wt PS-adobe
13 layer is summarized in Fig. 31.

14 It was found that the increase of the PS-adobe 8 thickness was accompanied by a noticeable
15 improvement of the green wall's time lag ranging between 5–10 h, meaning that the addition of 9
16 cm-tick of 8%wt PS-adobe into a double hollow brick can lead to design to a 0.23 hybrid wall
17 with a time lag of 10h. this finding is in a good agreement with the New Zealand standards that

1 estimates that a 0.28 m earth-based wall can achieve a time lag range of 7–10 h [58]. This
 2 increase in the time lag is attributed to the excellent thermal inertia of earth and the good thermal
 3 insulation of the incorporated mixture. It should also be noted that when 9 cm-thick PS-adobe 8
 4 was used instead of 1 cm-thick PS-adobe 8, the decrement factor was reduced by 87%,
 5 demonstrating the effectiveness of incorporating biosourced adobes in double hollow brick walls
 6 in regulating the indoor temperature fluctuations of buildings.

7 These findings lie in the range of values obtained in other bio-based adobe-related studies that
 8 showed that the time lag of 0.22 m adobe walls can achieve 4.63 h [59]. For 0.5 m adobe walls,
 9 this value can range between 13.7– 17.8 h [60] and 15.4–17.2 h [61], and 20.4–23.0 h [50]. All
 10 these results confirm the efficacy of the proposed hybrid wall configuration (hollow brick/earth)
 11 in insuring a good time lag of up to 10 h with a small thick wall of 0.23 m, especially compared
 12 to homogeneous walls that can reach a time lag range of 3.87–9.01 h [50].



13
 14

Fig. 31. Thermal performance of green wall versus PS-adobe 8 thickness.

1 **5 Discussion and future perspectives**

2 Besides sustainability, both experimental and numerical results demonstrated the efficacy of
3 employing bio-based earth layers within structural walls to improve thermal insulation and time
4 lag property of buildings. Several studies have proposed structural wall layouts for new
5 constructions and retrofitting applications in the literature [62-65]. Recently, Ben Zaid et al. [65]
6 experimentally investigated the potential use of Phase change material (PCM) panels to improve
7 the energy efficiency of clay-straw wall buildings located in a semi-arid Moroccan climate. The
8 optimal position of the PCM panels was also investigated. The results showed that the use of 5-
9 mm PCM panels on the inner wall surface can significantly improve the time delay and the
10 thermal storage performance, and reduce the indoor surface temperature by 3°C. Earlier Kong et
11 al. [62] investigated the optimum position of PCM-panels for retrofitting a 240-mm thick wall
12 constructed of perforated bricks. The study showed that applying PCM-panels on the inner or
13 outer surface of the exterior walls can increase the building time lag by 3 h and 2.1 h,
14 respectively. Similar results were reported in this work when a 5-cm air gap was replaced with a
15 bio-based earth layer (see Fig. 28), which resulted in a 3h improvement of the time delay in heat
16 transfer. Despite the small thickness of PCM panels, the use of bio-based earth blocks within the
17 building envelope seems to be the most accessible and cost-effective solution in underdeveloped
18 countries and rural areas.

19 Regarding recent studies related to masonry structures, many attempts have been made in the last
20 decade to simulate the performance of eco-efficient multi-layered structures in order to design
21 appropriate sustainable wall systems taking into account the French standard NF EN 1745 [66].
22 The latter standard is commonly adopted in masonry structure research, which gives the design
23 thermal conductivity of masonry structures based on their density and geometry (cavities, etc.).

1 Kyriakidis et al. [67] established a comparative multi-criteria framework to evaluate the overall
2 both thermal and environmental performance of modular multilayer construction structures based
3 on tabulated data reported in NF EN 1745 [66]. In addition, same authors [63] investigated the
4 energy performance of structural wall systems in Southern Europe. The findings highlighted the
5 low carbon footprint of traditional earthen structures and the importance of retrofitting to
6 enhance the thermal performance of existing buildings. The authors also reported that the
7 thermal conductivity value of adobes according to NF EN 1745 is about 0.7 W/mK, which is in
8 good agreement with the value obtained in this work using the hot disk method.

9 Considering the NF EN 1745 standard [66], masonry structures are characterized by another
10 important property called the thermal transmittance *U-value*, which characterizes the overall
11 thermal performance of simple and multi-layer walls. Laaroussi et al. [41] numerically
12 investigated and compared the thermal resistance and the U-value of the 8-hole bricks used in the
13 proposed hybrid wall case study with the values obtained according to NF EN 1745 [66]. They
14 found a good agreement with a deviation of less than 3%. Moreover, the Moroccan building
15 energy code (RTCM) devolved by the Moroccan Agency of energy efficiency has implemented
16 an easy-to-use software (called “BINAYATE Prescriptive”) to help construction professionals in
17 designing thermally compliant structure based on the U-value property [68]. It should be mention
18 that BINAYATE Prescriptive tool constitutes of a thermophysical database of building materials
19 marketed on the national market, characterized according to NF EN 1745 standard [66]. By using
20 BINAYATE software, the thermal transmittance of a multilayer wall can be determined easily
21 from the following expression [68]:

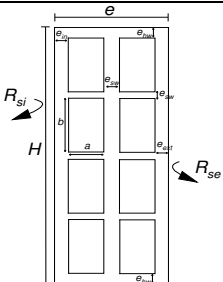
$$U_{wall} = \frac{1}{R_{se} + \sum \frac{e_i}{\lambda_i} + \sum R_j} \quad (15)$$

1 Where λ_i and e_i are respectively the thermal conductivity (W/mK) and the thickness (m) of the
 2 ith material constituting the wall, R_j is the thermal resistance of the jth constructing layer, R_{se} is
 3 the external surface resistance (0.04 m²K/W), R_{si} is the internal surface resistance (0.13
 4 m²K/W). Both values of the thermal surface resistances (i.e. R_{si} and R_{se}) are taken in accordance
 5 with NF EN 1745 standard [66].

6 Table 8 gives the thermal transmittance and the design thermal resistance of masonry structures
 7 of different walls studied. The results showed that that the BIANAYTE Prescriptive software's
 8 values are in good agreement with those reported in the literature. Furthermore, Table 8 clearly
 9 showed that replacing air gap with a bio-based earth layer can greatly improve the overall
 10 thermal transmittance of the building envelope, which will be advantageous in reducing the
 11 annual energy consumption of buildings.

12 Note that the dimensions of the 8-hole brick shown in Table 8 are the same as those used in our
 13 CFD study.

14 **Table 8.** Thermal transmittance and the design thermal resistance of masonry structures of
 15 different studied walls (according to NF EN 1745)

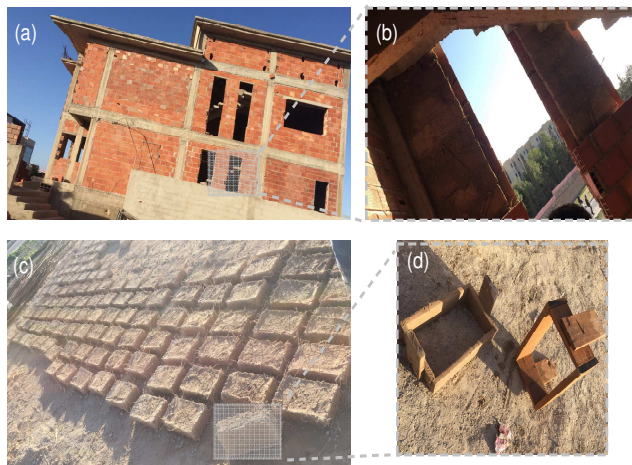
Masonry structure	Description	R_{th} (m ² K/W)	U (W/m ² K)
8-hole bricks (e=6.8 cm) <i>Present</i> Laaroussi et al. [41] CSTB [69]		0.358	1.89
		0.350	1.90
		0.370	1.85
8-hole bricks (e=7 cm) <i>Present</i>		0.368	1.86
Typical wall (e= 23 cm) <i>Present</i>	8-hole bricks (7 cm)	0.368	0.92
	Air gap (9 cm)	0.180	
	8-hole bricks (7 cm)	0.368	
Hybrid bio-based wall (e= 23 cm) <i>Present</i>	8-hole bricks (7 cm)	0.368	0.85
	PS-adobes 8wt% (9 cm)	0.270	

	8-hole bricks (7 cm)	0.368	
--	----------------------	-------	--

e : Thickness of the wall, H : the height of the brick (0.002 m), R_{si} and R_{se} are respectively the internal and external surface resistance ($R_{se} + R_{si} = 0.13 \text{ m}^2\text{K/W}$ [66]), $a=0.021 \text{ m}$, $b=0.041 \text{ m}$, $e_{hw}=0.009 \text{ m}$, $e_{ext}=0.01 \text{ m}$, $e_{in}=0.01 \text{ m}$.

1 In terms of future perspectives, a demonstrative building (Fig. 32) is underway to assess the
 2 effectiveness of the proposed bio-based hybrid wall configuration in improving passive thermal
 3 comfort and reducing the annual energy bill of buildings located in semi-arid climates of
 4 Morocco. future work will focus on :

- 5 • The evaluation of the constructed building's energy consumption taking into account the
 6 occupancy behavior.
- 7 • The real time monitoring of the thermal comfort level and the occupants' satisfaction.
- 8 • The life cycle assessment and energy audit of the proposed construction practice taking into
 9 account Morocco's various climate zones.



10

11 **Fig. 32.** Photographs of the demonstrative building constructed with the proposed bio-based
 12 hybrid wall (a) construction underway (b) exterior walls (c) adobes developed on site (d)
 13 molds used.

14 **6 Conclusion**

1 This study proposes a new and green construction technique for the use of highly biosourced
2 adobes in modern buildings. The paper begins by investigating the thermal and mechanical
3 performance of biosourced adobes produced from a local clayey soil with different weight
4 fractions of 0, 2, 4, 6 and 8% of Pennisetum Setaceum fibers. Prior to sample preparation, the
5 identification tests of raw materials were carried out by investigating the geotechnical, chemical
6 and morphological characteristics. The results show that the soil has good geotechnical and
7 particle size properties for adobe manufacturing, with a clay content of 48.5 %. On the other
8 hand, the potential use of Pennisetum setaceum (PS) fiber as a pore-forming agent for improving
9 the thermal insulation property of adobes was confirmed using scanning electron microscopy.
10 The X-ray diffraction analysis also indicates that PS fibers composed of a high cellulose content
11 that can be advantageous in the design of efficient earth masonry units.

12 The laboratory testing of produced PS-adobes show that the clay used exhibit low mechanical
13 strength of 1.7 MPa and a thermal conductivity value of $0.77 \text{ W}\cdot\text{m}^{-1}\cdot\text{K}^{-1}$. It was found that the
14 increasing incorporation of PS fibers improves the thermal transport properties and reduces the
15 mechanical strength of adobe. Adding 8%wt of PS fibers can improve the thermal conductivity
16 and the specific heat capacity of adobe by 6.7% and 17.9%, respectively. Moreover, the results
17 show that adobes with 8%wt of PS fibers can delay heat transfer by 45.8% compared to adobe
18 alone, which could be effective for moderating indoor temperature fluctuations in buildings.

19 In order to tackle the low mechanical properties of high bio-content adobes, a wall-scale
20 performance analysis of a hybrid bio-based wall configuration composed of a double hollow
21 brick wall incorporated by an 8%wt adobe layer using a CFD method. A comparative study on
22 the impact of adobes' thickness on the thermal performance of proposed wall system was
23 considered. The thermal performance was evaluated based on the time lag and the decrement

1 factor indexes. The findings results demonstrate the effectiveness of the hybrid biosourced wall
2 (brick/PS-adobe/brick) in regulating the indoor conditions due to its high thermal mass and
3 insulation compared to typical walls (brick/air gap/brick). A time lag improvement of 3h was
4 observed when replacing air gap by the PS-adobe layer. Moreover, it was found that the
5 incorporation of 9-cm-thick PS-adobe layer into a double hollow brick wall can lead to designing
6 lightweight high performance walls with a 10-h time lag. Based on these results, we can
7 conclude that the integration of high-biosourced earth masonry into the building envelope is a
8 promising technique for eco-construction and the design of high performance lightweight walls
9 compatible with the requirements of modern buildings.

10 **Acknowledgment**

11 Mouatassim Charai would like to thank the Director of ARGILUX Company, Mr. Ibrahim El
12 Eulj, for his cooperation and industrial partnership. Mouatassim Charai would also thank
13 Professor Elkader Gharibi and Dr. Hicham Nasri, respectively, for providing the glass blades and
14 helping to discuss X-ray diffraction spectra.

15 The authors would like to thank the Moroccan ‘National Center for Scientific and Technical
16 Research’ (996183890) for funding this work through the PPR project ‘Promotion of solar
17 energy and energy efficiency in the oriental region of Morocco’.

18 **A Tribute to Professor Kamal EL Hammouti**

19 This work was not finished without Professor Kamal EL Hammouti, Professor at the Laboratory
20 of Applied Geosciences at the faculty of sciences of Mohammed the first University, which has
21 recently passed away due to COVID19. Our sincere and heartfelt condolences go out to his
22 family, friends and colleagues.

1 **Declaration of interest**

2 The authors declare no conflict of interests.

1 **References**

- 2 [1] Z. Zhang, Y.C. Wong, A. Arulrajah, S. Horpibulsuk, A review of studies on bricks using alternative
3 materials and approaches, *Constr. Build. Mater.* 188 (2018) pp. 1101-1118.
4 <https://doi.org/10.1016/j.conbuildmat.2018.08.152>.
- 5 [2] A. Laborel-Preneron, J.-E. Aubert, C. Magniont, C. Tribout, A. Bertron, Plant aggregates and fibers in
6 earth construction materials: A review, *Constr. Build. Mater.* 111 (2016) pp. 719-734.
7 <https://doi.org/10.1016/j.conbuildmat.2016.02.119>.
- 8 [3] M.A. Bahobail, The mud additives and their effect on thermal conductivity of adobe bricks, *J. Eng.*
9 *Sci.* 40(1) (2012) pp. 21-34. <https://doi.org/10.21608/jesaun.2012.11271>.
- 10 [4] C. Galán-Marín, C. Rivera-Gómez, J. Petric, Clay-based composite stabilized with natural polymer
11 and fibre, *Constr. Build. Mater.* 24 (8) (2010) 1462-1468.
12 <https://doi.org/10.1016/j.conbuildmat.2010.01.008>.
- 13 [5] A. Schicker, S. Gier, Optimizing the mechanical strength of adobe bricks, *Clay and Clays Minerals*,
14 57(4) (2009) pp. 494-501. <https://doi.org/10.1346/CCMN.2009.0570410>.
- 15 [6] S.Z. Salleh, A.A. Kechik, A.H. Yusoff, M.A.A. Taib, M.M. Nor, M. Mohamad, T.G. Tan, A. Ali,
16 M.N. Masri, J.J. Mohamed, Recycling Food, Agricultural, and Industrial Wastes as Pore-Forming Agents
17 for Sustainable Porous Ceramic Production: A Review, *J clean. Prod.* 306 (2021) p. 127264.
18 <https://doi.org/10.1016/j.jclepro.2021.127264>.
- 19 [7] K.-Y. Chiang, P.-H. Chou, C.-R. Hua, K.-L. Chien, C. Cheeseman, Lightweight bricks manufactured
20 from water treatment sludge and rice husks, *J. Hazard. Mater.* 171 (2009) pp. 76-82.
21 <https://doi.org/10.1016/j.jhazmat.2009.05.144>.
- 22 [8] F. Jové-Sandoval, M.M. Barbero-Barrera, N.F. Medina, Assessment of the mechanical performance
23 of three varieties of pine needles as natural reinforcement of adobe, *Constr. Build. Mater.* 187 (2018) pp.
24 205-213. <https://doi.org/10.1016/j.conbuildmat.2018.07.187>.

- 1 [9] L. Ba, I. El Abbassi, T.-T. Ngo, P. Pliya, C.S.E. Kane, A.-M. Darcherif, M. Ndongo, Experimental
2 Investigation of Thermal and Mechanical Properties of Clay Reinforced with *Typha australis*: Influence
3 of Length and Percentage of Fibers, *Waste Biomass Valor.* 12 (2021) pp. 2723-2737.
4 <https://doi.org/10.1007/s12649-020-01193-0>.
- 5 [10] F. El Fgaier, Z. Lafhaj, F. Brachelet, E. Antczak, C. Chapiseau, Thermal performance of unfired
6 clay bricks used in construction in the north of France: Case study, *Case Stud Constr. Mater.* 3 (2015) pp.
7 102-111. <https://doi.org/10.1016/j.cscm.2015.09.001>.
- 8 [11] M. Beccali, V. Strazzeri, M. Germanà, V. Melluso, A. Galatioto, Vernacular and bioclimatic
9 architecture and indoor thermal comfort implications in hot-humid climates: An overview, *Renew.*
10 *Sustain. Energy Rev.* 82 (2018) pp. 1726-1736. <https://doi.org/10.1016/j.rser.2017.06.062>.
- 11 [12] M.E. Mallea, L.E. Igiñiz, M.d.L.G. de Diego, Environment, Passive hygrothermal behaviour and
12 indoor comfort concerning the construction evolution of the traditional Basque architectural model. Lea
13 valley case study, *Build. Environ.*, 143 (2018) pp. 496-512.
14 <https://doi.org/10.1016/j.buildenv.2018.06.041>.
- 15 [13] L. Zhang, G. Sang, W. Han, Effect of hygrothermal behaviour of earth brick on indoor environment
16 in a desert climate, *Sustain. Cities Soc.* 55 (2020) 102070. <https://doi.org/10.1016/j.scs.2020.102070>.
- 17 [14] A.W. Bruno, D. Gallipoli, C. Perlot, H. Kallel, Thermal performance of fired and unfired earth
18 bricks walls, *J. Build. Eng.* 28 (2020) p. 101017. <https://doi.org/10.1016/j.job.2019.101017>.
- 19 [15] M.S. Zami, A. Lee, Economic benefits of contemporary earth construction in low-cost urban
20 housing—state-of-the-art review, *J. Build. Apprais.* 5 (2010) pp. 259-271.
21 <https://doi.org/10.1057/jba.2009.32>.
- 22 [16] D. Medjelekh, L. Ulmet, F. Gouny, F. Fouchal, B. Nait-Ali, P. Maillard, F. Dubois, Characterization
23 of the coupled hygrothermal behaviour of unfired clay masonries: Numerical and experimental aspects, .
24 *Build. Environ.* 110 (2016) pp. 89-103. <https://doi.org/10.1016/j.buildenv.2016.09.037>.

- 1 [17] Haut Commissariat au Plan, Monographie de la Région de l'Orientale.
2 <https://www.hcp.ma/region-oriental/docs/Monographies/,2021>
3 (accessed 9 July 2021)..
- 4 [18] H.N. Le Houérou, Bioclimatologie et biogéographie des steppes arides du Nord de
5 l'Afrique, Centre international de hautes études agronomiques méditerranéennes, Options
6 Méditerranéennes, Montpellier, France (1995). <http://om.ciheam.org/om/pdf/b10/CI951183.pdf>.
- 7 [19] ISO 17892-4 , Geotechnical investigation and testing — Laboratory testing of soil — Part 4:
8 Determination of particle size distribution, (2016).
- 9 [20] NF P94-051, Sols : reconnaissance et essais - Détermination des limites d'Atterberg - Limite de
10 liquidité à la coupelle - Limite de plasticité au rouleau, (1993).
- 11 [21] M. Charai, H. Sghiouri, A. Mezrhab, M. Karkri, K. El Hammouti, Comparative study of a clay
12 before and after fired brick-making process, Mater. Today: Proc. 31 (2020) S103-S108.
13 <https://doi.org/10.1016/j.matpr.2020.06.250>.
- 14 [22] M. Trindade, M. Dias, F. Rocha, M. Prudêncio, J. Coroado, Bromine volatilization during firing of
15 calcareous and non-calcareous clays: archaeometric implications, Appl. Clay Sci. 53 (2011) pp. 489-499.
16 <https://doi.org/10.1016/j.clay.2010.07.001>.
- 17 [23] J. Yvon, P. Garin, J. Delon, J.M. Cases, Valorisation des argiles kaolinitiques des Charentes dans le
18 caoutchouc naturel, Bull. Minér. 105 (1982) pp. 431-437..
- 19 [24] N.A. Yusoff, M.F.M. Fauzi, F. Abdullah, The study of soil-roots strength performance by using
20 Pennisetum setaceum grass, MATEC Web Conf. 47 (2016) p. 03021.
21 <https://doi.org/10.1051/mateconf/20164703021>.
- 22 [25] V.N. Nkemka, Y. Li, X. Hao, Technology, Effect of thermal and alkaline pretreatment of giant
23 miscanthus and Chinese fountaingrass on biogas production, Water Sci Technol, 73 (2016) pp. 849-856.
24 <https://doi.org/10.2166/wst.2015.559>.

- 1 [26] S. Milton, W. Dean, S.J. Rahlao, Evidence for induced pseudo-vivipary in *Pennisetum setaceum*
2 (Fountain grass) invading a dry river, arid Karoo, South Africa, *S. Afric. J. Bot.* 74 (2008) pp. 348-349.
3 <https://doi.org/10.1016/j.sajb.2007.11.012>.
- 4 [27] S. Park, J.O. Baker, M.E. Himmel, P.A. Parilla, D.K. Johnson, Cellulose crystallinity index:
5 measurement techniques and their impact on interpreting cellulase performance, *Biotechnol. Biofuels.* 3
6 (2010) 10. <https://doi.org/10.1186/1754-6834-3-10>.
- 7 [28] L. Segal, J. Creely, A. Martin Jr, C. Conrad, An empirical method for estimating the degree of
8 crystallinity of native cellulose using the X-ray diffractometer, *Tex. Res. J.* 29 (1959) pp. 786-794.
9 <https://doi.org/10.1177/004051755902901003>.
- 10 [29] D. Dai, M. Fan, Characteristic and performance of elementary hemp fibre, *Mater. Sci.*
11 *Appl.* 1 (2010) pp. 336-342. <https://doi.org/10.4236/msa.2010.16049>.
- 12 [30] H. Yang, R. Yan, H. Chen, D.H. Lee, C.J. Zheng, Characteristics of hemicellulose, cellulose and
13 lignin pyrolysis, *Fuel.* 86 (2007) pp. 1781-1788. <https://doi.org/10.1016/j.fuel.2006.12.013>.
- 14 [31] M. Ouedraogo, K. Dao, Y. Millogo, J.-E. Aubert, A. Messan, M. Seynou, L. Zerbo, M. Gomina,
15 Physical, thermal and mechanical properties of adobes stabilized with fonio (*Digitaria exilis*) straw, *J.*
16 *Build. Eng.* 23 (2019) pp. 250-258. <https://doi.org/10.1016/j.jobe.2019.02.005>.
- 17 [32] O. Ige, H. Danso, Physico-mechanical and thermal gravimetric analysis of adobe masonry units
18 reinforced with plantain pseudo-stem fibres for sustainable construction, *Constr. Build. Mater.* 273 (2021)
19 p. 121686. <https://doi.org/10.1016/j.conbuildmat.2020.121686>.
- 20 [33] Y. Millogo, J.-C. Morel, J.-E. Aubert, K. Ghavami, Experimental analysis of Pressed Adobe Blocks
21 reinforced with *Hibiscus cannabinus* fibers, *Constr. Build. Mater.* 52 (2014) pp. 71-78.
22 <https://doi.org/10.1016/j.conbuildmat.2013.10.094>.

- 1 [34] G. Araya-Letelier, F. Antico, C. Burbano-Garcia, J. Concha-Riedel, J. Norambuena-Contreras, J.
2 Concha, E.S. Flores, Experimental evaluation of adobe mixtures reinforced with jute fibers, *Constr.*
3 *Build. Mater.* 276 (2021) p. 122127. <https://doi.org/10.1016/j.conbuildmat.2020.122127>.
- 4 [35] ISO 22007-2, Plastics — Determination of thermal conductivity and thermal diffusivity — Part 2:
5 Transient plane heat source (hot disc) method, (2008).
- 6 [36] M. Madrid, A. Orbe, E. Roji, J. Cuadrado, The effects of by-products incorporated in low-strength
7 concrete for concrete masonry units, *Constr. Build. Mater.* 153 (2017) pp. 117-128.
8 <https://doi.org/10.1016/j.conbuildmat.2017.07.086>.
- 9 [37] XP-13-901 Compressed earth blocks fo walls and partitions : definitions - Specifications - Test
10 methods - Delivery acceptance conditions, (2001).
- 11 [38] G.A. Jokhio, F.M. Saad, Y. Gul, S.M.S. Mohsin, N.I. Ramli, Uniaxial compression and tensile
12 splitting tests on adobe with embedded steel wire reinforcement, *Constr. Build. Mater.* 176 (2018) pp.
13 383-393. <https://www.sciencedirect.com/science/article/pii/S0950061818310602>.
- 14 [39] NF EN 12390-6, Testing hardened concrete - Part 6 : tensile splitting strength of test specimens,
15 (2012).
- 16 [40] NF P94-078, Soils : investigation and tests. CBR after immersion. Immediate CBR. Immediate
17 bearing ratio. Measurement on sample compacted in CBR mould, (1997).
- 18 [41] N. Laaroussi, G. Lauriat, S. Raefat, M. Garoum, M. Ahachad, An example of comparison between
19 ISO Norm calculations and full CFD simulations of thermal performances of hollow bricks, *J. Build. Eng.*
20 11 (2017) pp. 69-81. <https://doi.org/10.1016/j.jobe.2017.03.011>.
- 21 [42] A. Gagliano, F. Nocera, S. Aneli, Thermodynamic analysis of ventilated façades under different
22 wind conditions in summer period, *Energy Build.* 122 (2016) pp. 131-139.
23 <https://doi.org/10.1016/j.enbuild.2016.04.035>.

- 1 [43] M. Mahdaoui, S. Hamdaoui, A.A. Msaad, T. Kousksou, T. El Rhafiki, A. Jamil, M. Ahachad,
2 Building bricks with phase change material (PCM): Thermal performances, *Constr. Build. Mater.* 269
3 (2021) p. 121315. <https://doi.org/10.1016/j.conbuildmat.2020.121315>.
- 4 [44] S. Dabiri, M. Mehrpooya, E.G. Nezhad, Latent and sensible heat analysis of PCM incorporated in a
5 brick for cold and hot climatic conditions, utilizing computational fluid dynamics, *Energy*. 159 (2018) pp.
6 160-171. <https://doi.org/10.1016/j.energy.2018.06.074>.
- 7 [45] D. Kizildag, I. Rodríguez, A. Oliva, O. Lehmkuhl, Limits of the Oberbeck–Boussinesq
8 approximation in a tall differentially heated cavity filled with water, *Int. J. Heat Mass. Transfer*. 68 (2014)
9 pp. 489-499. <https://doi.org/10.1016/j.ijheatmasstransfer.2013.09.046>.
- 10 [46] AMEE, Agence Marocaine pour l'Efficacité Energétique. Propriété thermo-physique des matériaux
11 locaux de construction au Maroc, (2017).
- 12 [47] R. Fathipour, A. Hadidi, Analytical solution for the study of time lag and decrement factor for
13 building walls in climate of Iran, *Energy* 134 (2017) pp. 167-180.
14 <https://doi.org/10.1016/j.energy.2017.06.009>.
- 15 [48] Y. Abu-Zidan, P. Mendis, T. Gunawardena, Optimising the computational domain size in CFD
16 simulations of tall buildings, *Heliyon* 7(4) (2021) e06723. <https://doi.org/10.1016/j.heliyon.2021.e06723>.
- 17 [49] Y. Abu-Zidan, P. Mendis, T. Gunawardena, Impact of atmospheric boundary layer inhomogeneity in
18 CFD simulations of tall buildings, *Hilyon* 6(7) (2020) e04274.
19 <https://doi.org/10.1016/j.heliyon.2020.e04274>.
- 20 [50] E. Malaktou, I. Ioannou, M. Philokyrou, Investigating the thermal properties of earth-based
21 materials: the case of adobes, M. Kouï, F. Zezza, D. Kouï (Eds.), *Proceedings of the 10th International*
22 *Symposium on the Conservation of Monuments in the Mediterranean Basin, Natural and Anthropogenic*
23 *Hazards and Sustainable Preservation*, Springer Cham (2017) pp. 95-103. <https://doi.org/10.1007/978-3->
24 [319-78093-1_9](https://doi.org/10.1007/978-3-319-78093-1_9).

- 1 [51] M. Achenza, L. Fenu, Structures, On earth stabilization with natural polymers for earth masonry
2 construction, *Mater. Struct.* 39(1) (2006) pp. 21-27. <https://doi.org/10.1617/s11527-005-9000-0>.
- 3 [52] H. Danso, D.B. Martinson, M. Ali, J.B. Williams, Physical, mechanical and durability properties of
4 soil building blocks reinforced with natural fibres, *Constr. Build. Mater.* 101 (2015) pp. 797-809.
5 <https://doi.org/10.1016/j.conbuildmat.2015.10.069>.
- 6 [53] D. Khoudja, B. Taallah, O. Izemmouren, S. Aggoun, O. Herihiri, A. Guettala, Mechanical and
7 thermophysical properties of raw earth bricks incorporating date palm waste, *Constr. Build. Mater.* 270
8 (2021) p. 121824. <https://doi.org/10.1016/j.conbuildmat.2020.121824>.
- 9 [54] B. Mazhoud, F. Collet, S. Prétot, C. Lanos, Effect of hemp content and clay stabilization on hygric
10 and thermal properties of hemp-clay composites, *Constr. Build. Mater.* 300 (2021) p. 123878.
11 <https://doi.org/10.1016/j.conbuildmat.2021.123878>.
- 12 [55] G. Guglielmini, U. Magrini, E. Nannei, The influence of the thermal inertia of building structures on
13 comfort and energy consumption, *J. Build. Phys.* 5(2) (1981) pp. 59-72.
14 <https://doi.org/10.1177/109719638100500201>.
- 15 [56] A. Brambilla, J. Bonvin, F. Flourentzou, T. Jusselme, On the influence of thermal mass and natural
16 ventilation on overheating risk in offices, *Buildings* 8 (2018) p. 47.
17 <https://doi.org/10.3390/buildings8040047>.
- 18 [57] V. Cheng, E. Ng, B. Givoni, Effect of envelope colour and thermal mass on indoor temperatures in
19 hot humid climate, *Solar Energy* 78(4) (2005) pp. 528-534. <https://doi.org/10.1016/j.solener.2004.05.005>.
- 20 [58] New Zealand Standard (NZS), Engineering design of earth buildings. NZS No. 4297. New Zealand
21 Standard, Wellington (1998).
- 22 [59] I. Neya, D. Yamegueu, Y. Coulibaly, A. Messan, A.L.S.-N. Ouedraogo, Impact of insulation and
23 wall thickness in compressed earth buildings in hot and dry tropical regions, *Build. Eng.* 33 (2021) p.
24 101612. <https://doi.org/10.1016/j.jobbe.2020.101612>.

- 1 [60] M. Moevus, R. Anger, L. Fontaine, Hygro-thermo-mechanical properties of earthen materials for
2 construction: a literature review, M. Correia, P. Jerome, M. Blondet, M. Achenza (Eds.), Proceedings of
3 the Terra 2012 conference, (2012).
- 4 [61] H. Guillaud, H. Houben , Earth construction: A comprehensive guide, (1994).
- 5 [62] X. Kong, S. Lu, J. Huang, Z. Cai, S. Wei, Experimental research on the use of phase change
6 materials in perforated brick rooms for cooling storage, *Energy Build.*, 62 (2013), pp. 597-604.
7 <https://doi.org/10.1016/j.enbuild.2013.03.048>.
- 8 [63] A. Kyriakidis, A. Michael, R. Illampas, D.C. Charnpis, I. Ioannou, Thermal performance
9 and embodied energy of standard and retrofitted wall systems encountered in Southern Europe,
10 *Energy*, 161 (2018), pp. 1016-1027. <https://doi.org/10.1016/j.energy.2018.07.124>.
- 11 [64] R. Bruno, C. Carpino, P. Bevilacqua, J. Settino, N. Arcuri, A novel Stay-In-Place
12 formwork for vertical walls in residential nZEB developed for the Mediterranean climate:
13 hygrothermal, energy, comfort and economic analyses, *J. Build. Eng.* 45 (2022) p. 103593.
14 <https://doi.org/10.1016/j.job.2021.103593>.
- 15 [65] Z. Ben Zaid, A. Tilioua, I. Lamaamar, O. Ansari, H. Souli, M.A.Hamdi Alaoui, An
16 experimental study of the efficacy of integrating a phase change material into a clay-straw wall
17 in the Drâa-Tafilalet Region (Errachidia Province), Morocco, *J. Build. Eng.* 32 (2020) p. 101670.
18 <https://doi.org/10.1016/j.job.2020.101670>.
- 19 [66] NF EN 1745, Masonry and masonry products - Methods for determining thermal properties
20 (2020).
- 21 [67] A. Kyriakidis, A. Michael, R. Illampas, D.C. Charnpis, I. Ioannou, Comparative evaluation
22 of a novel environmentally responsive modular wall system based on integrated quantitative and
23 qualitative criteria, *Energy*, 188 (2019), p. 115966.
24 <https://doi.org/10.1016/j.energy.2019.115966>.

- 1 [68] AMME, Agence Marocaine pour l'Efficacité Energétique, Règlement thermique de
2 Construction au Maroc (2014).
3 [https://www.amee.ma/sites/default/files/inline-
5 files/Reglement_thermique_de_construction_au_Maroc.pdf](https://www.amee.ma/sites/default/files/inline-
4 files/Reglement_thermique_de_construction_au_Maroc.pdf)
6 (accessed 4 January 2022).
- 7 [69] Etude de caractérisation thermophysique de briques rouges 6, 8 et 12 trous de la ville de
8 Salé, Rapport CSTB EMI 13-26046832, 2013.